# ACOUSTIC PROPAGATION IN A CONTINENTAL SLOPE OCEAN ENVIRONMENT

by

STANLEY EDWARD DOSSO
B.Sc., University of Victoria, 1982

A THESIS SUBMITTED IN PARTIAL FULFILLMENT
OF THE REQUIREMENTS FOR THE DEGREE OF
MASTER OF SCIENCE
in the Department
of
Physics

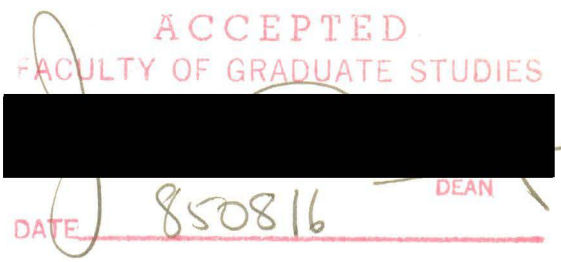


We accept this thesis as conforming
to the required standard

[redacted]
N.R. Chapman

[redacted]
J.T. Weaver

[redacted]
R.M. Clements

[redacted]
D.E. Hewgill

[redacted]
L.A. Hobson

Supervisors: Dr. N.R. Chapman and Dr. J.T. Weaver

## ABSTRACT

The analysis and interpretation of experiments carried out to study acoustic propagation in a continental slope ocean environment are presented in this thesis. Measurements of the propagation loss in 1/3-octave bands from 25 to 630 Hz were obtained for propagation both up and down the continental slope in experiments off the west coast of Vancouver Island. The propagation was strongly influenced by the ocean floor bathymetry. A slope enhancement effect (decreasing loss with range) was observed for sound propagating down the continental slope. The maximum enhancement occurred for sources near the edge of the continental shelf, with measured losses as much as 16 dB less than those estimated for propagation over a flat ocean bottom. The slope enhancement effect was greatest at the high frequencies. In contrast, large losses were measured for propagation up the continental slope, particularly at high frequencies. The propagation loss for sources near the base of the slope exceeded that estimated for a flat ocean bottom by as much as 15 dB.

The parabolic equation method, which is well suited to modelling low-frequency propagation in a range-dependent environment, was used to model both the downslope and upslope propagation measurements. A treatment of the effects of density variations in the sub-bottom layers was added to the model in this thesis. The results of several test cases indicate that this addition leads to significant improvements in the model predictions. The losses calculated for propagation down the slope were in excellent agreement with the experimentally measured values. The model calculations for propagation up the slope exhibited the correct range-dependent behavior, but differed in level from the measured values which include losses

due to three-dimensional effects that cannot be accounted for by the model used in this work. These results indicate that the "variable-density" parabolic equation method can accurately model the acoustic propagation in a continental slope environment.

[redacted]
N.R. Chapman

[redacted]
J.T. Weaver

[redacted]
R.M. Clements

[redacted]
D.W. Hewgill

[redacted]
L.A. Hobson

# ACOUSTIC PROPAGATION IN A CONTINENTAL SLOPE OCEAN ENVIRONMENT

## TABLE OF CONTENTS

# LIST OF TABLES

# LIST OF FIGURES

FIGURE Page

FIGURE Page

FIGURE Page

## ACKNOWLEDGEMENTS

I would like to thank my supervisors Dr. N.R. Chapman and Dr. J.T. Weaver for their valuable assistance and guidance in this research. I would also like to express my appreciation for the use of facilities and the support of the staff at the Defence Research Establishment Pacific. The financial support of N.S.E.R.C. scholarships and the R.M. Pearce Memorial Fellowship is gratefully acknowledged.

# CHAPTER 1
# INTRODUCTION

## 1.1 Acoustic Propagation in the Ocean

Underwater acoustics is an important field of study that has been developed extensively in the last forty years in response to practical needs. Since electromagnetic radiation such as light and radio waves is strongly attenuated in the ocean, the efficient propagation of sound to long ranges has been exploited with diverse applications such as depth sounding and side-scan sonar, the detection of surface ships and submarines, telemetry and communications, seismic profiling of the ocean bottom, and the measurement of ocean currents and temperature structure. In order to use sound as a tool in the ocean, the manner in which it propagates must be understood.

The first modern scientific paper on underwater sound was published by Lichte (1919) describing the refraction of sound by slight temperature and salinity gradients in shallow waters. In the 1920's, however, very little attention was given to understanding acoustic propagation in the ocean. Efforts were directed almost exclusively to the development of sound projectors and receivers for echo ranging. By the early 1930's it was apparent that the ranges being obtained with the newly developed equipment were extremely variable, and that this variability must somehow be due to the properties of the ocean itself. The use of sensitive thermometers placed at close intervals along a wire and the mechanical bathythermograph, developed in 1937, demonstrated the existence of sufficient temperature gradients in the near surface waters to refract sound from a shallow source into the ocean depths. World War II provided the impetus for intensive research and development in the field of underwater acoustics. The existence and propagation characteristics of the deep sound channel were discovered (Ewing and Worzel, 1948) and used in submarine detection and in establishing a SOFAR (sound fixing and ranging) system in the Pacific Ocean to locate acoustically aviators downed at sea (Stiffler,

1948). Long range propagation in the deep sound channel also made it possible to measure and identify attenuation effects in sea water. Klein (1968) and Lasky (1976) described in further detail the development of underwater acoustics prior to and during the Second World War.

The field of underwater acoustics has continued to grow rapidly since the War (Urick (1982) fitted an exponentially increasing curve to the number of papers published per year since 1950). Some of the major accomplishments in the last 30 years are summarized by Urick (1982), and include: an understanding of the propagation characteristics and losses in the deep sound channel, measurements of bottom loss in many deep-water areas, the discovery of excess attenuation due to chemical relaxation processes at frequencies below 1 kHz, and the development of numerical ray and wave-theory models.

An important field of current research continues to be the study of acoustic propagation in a range-dependent ocean environment (i.e. an environment involving horizontal variations in acoustically-important parameters). Propagation studies generally involve experimental measurements at sea or the use of numerical models implemented on a computer. Measurements at sea are normally carried out using two ships: a source ship and a receiving ship. The receiving ship records the acoustic signals from underwater sources deployed at different ranges by the source ship. Experimental measurements are expensive to carry out and the results may be difficult to interpret because the environment may not be known completely. Numerical studies attempt to model the propagation by solving the wave equation (or some approximation to it) for the environment of interest. Although such studies are relatively inexpensive to carry out, the results may be of little more than academic interest unless the physical model of the ocean environment is realistic.

A particular problem of theoretical and practical importance is that of acoustic propagation in a "wedge-shaped ocean" (i.e. an ocean with a sloping bottom). Historically, the problem of radiation fields in wedges has been considered theoretically since the late nineteenth century (Sommerfeld 1894, 1896). In a more practical sense, it is important to understand acoustic propagation in the continental slope regions which border all coastlines. Although the problem has received theoretical attention and several modelling studies have been carried out for idealized slope environments in recent years, few experimental measurements have been reported for continental slope regions.

Understanding acoustic propagation in a continental slope environment involves two distinct problems: sound propagating either up or down the slope. In either case the propagation is strongly influenced by the variation in ocean depth with range. Officer (1958) first described propagation in an ocean with sloping floor. Acoustic rays (normals to the propagating wavefronts) traverse the slope by a series of bottom and surface reflections. At each bottom reflection the grazing angle of the ray (measured with respect to the horizontal) is increased or decreased by twice the slope angle. In the case of propagation up a slope, the angle becomes steeper with each bottom reflection. Loss due to transmission into the bottom increases at each reflection as the grazing angle steepens, and eventually the ray essentially penetrates the bottom and propagates into the sediments. Graves et al. (1975), Jensen and Kuperman (1980) and Gilbert et al. (1983) have demonstrated this bottom penetration for an isovelocity, wedge-shaped ocean by plotting loss contours for the water column and underlying sediments. These loss values were calculated using a variety of numerical methods (adiabatic normal mode theory, a parabolic equation solution, and coupled mode theory, respectively). Buckingham (1983) states that a straightforward solution to the wave equation for a

wedge-shaped ocean with a penetrable bottom would seem to be impossible, and derives an approximate analytical solution for an isovelocity wedge with perfectly reflecting boundaries. He then modifies this to allow transmission into the bottom.

In the case of acoustic propagation down a slope, the grazing angle of the ray is reduced by twice the slope angle at each bottom reflection, resulting in less loss due to transmission into the ocean bottom at each successive reflection. If a sloping bottom is encountered at depths within the deep sound channel, the ray angle may be sufficiently reduced upon bottom reflection to become continuously refracted within the sound channel and propagate without further bottom interactions. This downslope conversion to low loss paths may result in a slope enhancement effect, that is, a decrease in measured loss with range. Northrop et al. (1968) detonated explosive sound sources in the shallow waters overlying the continental shelf off Point Arena, California and measured (broadband) signal levels in the deep sound channel near Eniwetok and Midway. They reported enhanced signal levels for sources over the continental slope, with a maximum level recorded for sources near the shelf edge. Wagstaff (1980) considered the importance of the downslope conversion of ship noise generated over the continental slope into the deep sound channel. Wales and Diachock (1981) observed a peak in the ambient noise field at small angles to the horizontal in measurements of the vertical directionality of noise near Bermuda. They attributed this to slope enhanced signals from near-shore shipping and demonstrated a slope enhancement effect for a simplified continental slope environment using a parabolic equation model. Koch et al. (1983) and Koch (1983) have carried out numerical studies of the sensitivity of upslope and downslope propagation to environmental parameters (sediment attenuation, density and sound speed, and slope angle) and to the source and receiver depth for a simplified continental slope environment using an adiabatic normal mode model.

## 1.2 Summary of Work in this Thesis

The purpose of the work reported in this thesis was to study acoustic propagation in a continental slope ocean environment. Experimental measurements of the propagation loss with range were carried out at sea in two locations off the west coast of Vancouver Island, British Columbia. The measurements were interpreted by considering the propagation paths predicted according to ray theory, and by examining the recorded acoustic signals in both the time and frequency domains. Propagation in the oceanographic environments recorded in the experiment was modelled numerically using the parabolic equation model of Thomson and Chapman (1983) which was extended in this thesis to include the effects of density variations in the sub-bottom layers.

# CHAPTER 2
# EXPERIMENTAL MEASUREMENT OF PROPAGATION LOSS

## 2.1 The Experimental Method

Measurement of the propagation loss with range, using small explosive charges as sound sources, is a well-established method of studying acoustic propagation in a particular environment (Chapman, 1983a; Chapman et al., 1983; Dosso and Chapman, 1983). The experimental method, known as a shot run, involves two ships: a source ship and a receiving ship. The receiving ship monitors an array of hydrophones while the source ship opens range from the receiving system and deploys sound sources at selected range intervals. From the measurements of acoustic pressure recorded at the hydrophones and a knowledge of the source levels, the propagation loss may be calculated for each source-receiver range.

The two ships used in the experiments described here were CFAV ENDEAVOUR and CSS PARIZEAU. CFAV ENDEAVOUR acted as the receiving ship and maintained position monitoring the MEVA (Multi-Element Volume Array) hydrophone system. The principal components of the MEVA system are shown in Fig. 2.1. The hydrophones were suspended below a surface buoy which was anchored at each station. The distributed buoyancy floats allow the submerged equipment to achieve neutral buoyancy and maintain slack in the cable leading to the surface buoy. This arrangement, together with the two-stage suspension system consisting of the large damper plate and the deep sub-surface float, ensures that the hydrophones are unaffected by any motion of the ocean surface. The hydrophones are arranged in a two-dimensional horizontal array and a vertical line array. A pressure sensor located in the horizontal array was used to determine the hydrophone

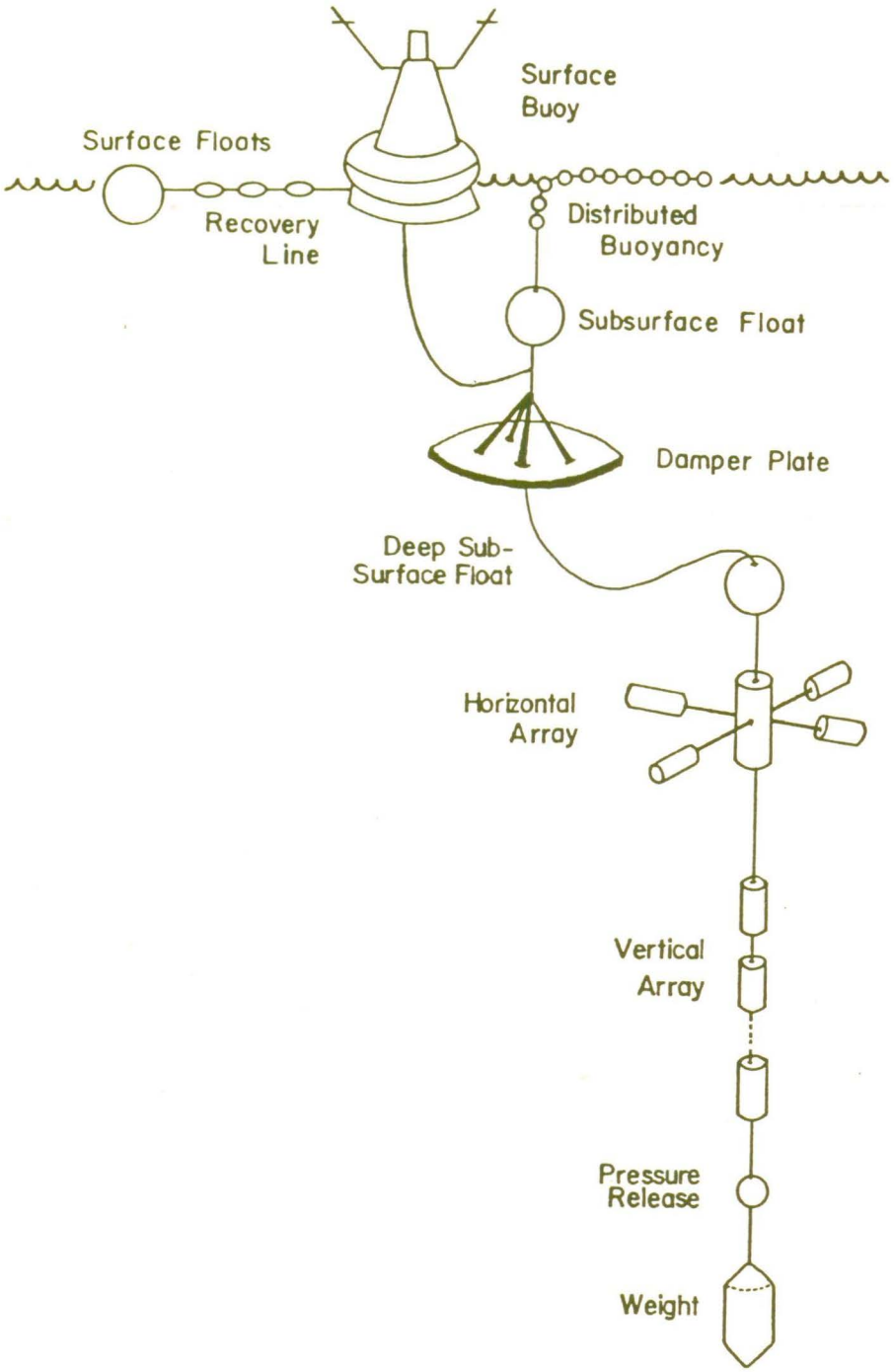


Fig. 2.1. The MEVA hydrophone system.

depths. The vertical array was suspended at a depth of about 400 - 600 m. The hydrophone signals were sampled at a rate of 1500 samples/s, and the digital signals were transmitted by a radio frequency telemetry link to the receiving ship for recording on magnetic tape. During the experiment, CFAV ENDEAVOUR maintained a distance of about 1 km from the MEVA system to avoid adding excessively to the ambient noise.

CSS PARIZEAU, acting as the source ship, opened range from the receiving system along a predetermined track, and dropped 0.82-kg SUS (Signal Underwater Sound) charges at 1.5 - 2.0 km range intervals. These charges, set to detonate at a depth of 22 m, provided the acoustic sources for the experiment. Coincident with detonation of the charges, a radio tone was transmitted from the source ship to the receiving ship to permit determination of the acoustic travel times.

The source ship also employed instruments to measure several properties of the oceanographic environment along the shot run track. Velocimeter casts were used to measure the sound-speed profiles to a depth of about 1000 m at each end of the track and expendable bathythermographs were used to measure the temperature profiles (from which sound-speed profiles can be inferred) to a depth of about 500 m at 25-km range intervals along the track. The sound-speed profiles may be extended to the ocean floor with the aid of historical data, since the properties of the deep ocean remain relatively constant. Continuous measurement of the bathymetry along the track was recorded using the 12-kHz echo-sounding sonar of the source ship. With the aid of Loran C and satelite navigation, the positions of both ships (latitude and longitude) were recorded regularly.

Measurments were carried out along two shot run tracks off the west coast of Vancouver Island, British Columbia. The receiving system locations and the source ship traverses are shown in Fig. 2.2. The tracks were selected to traverse the continental slope in regions where bathymetric charts indicated the slope was relatively regular and monatonic. In shot run 1 the receiving system was located at the deep-water end of the track and the source ship moved into progressively shallower water. This is known as a downslope propagation shot run, since the acoustic waves propagate down the slope to the receiver. In shot run 2 the receiving system was located at the shallow-water end of the track and the source ship moved into progressively deeper water. This is known as an upslope propagation shot run. Upslope and downslope propagation shot runs are shown schematically in Fig. 2.3.

## 2.2 Calculation of Propagation Loss

The total acoustic flux density $E_T$ at a range r from a source of a pressure disturbance in a medium of density $\rho$ and sound speed c is

$$E_T(r) = \frac{1}{\rho c} \int_{-\infty}^{\infty} p^2(t)dt \quad , \tag{2.1}$$

where p(t) is the total pressure disturbance at r, due to the source and the ambient noise n(t). According to Parseval's theorem, $E_T$ may be expressed as

$$E_T(r) = \frac{1}{2\pi\rho c} \int_{-\infty}^{\infty} |P(\omega)|^2 d\omega \quad , \tag{2.2}$$

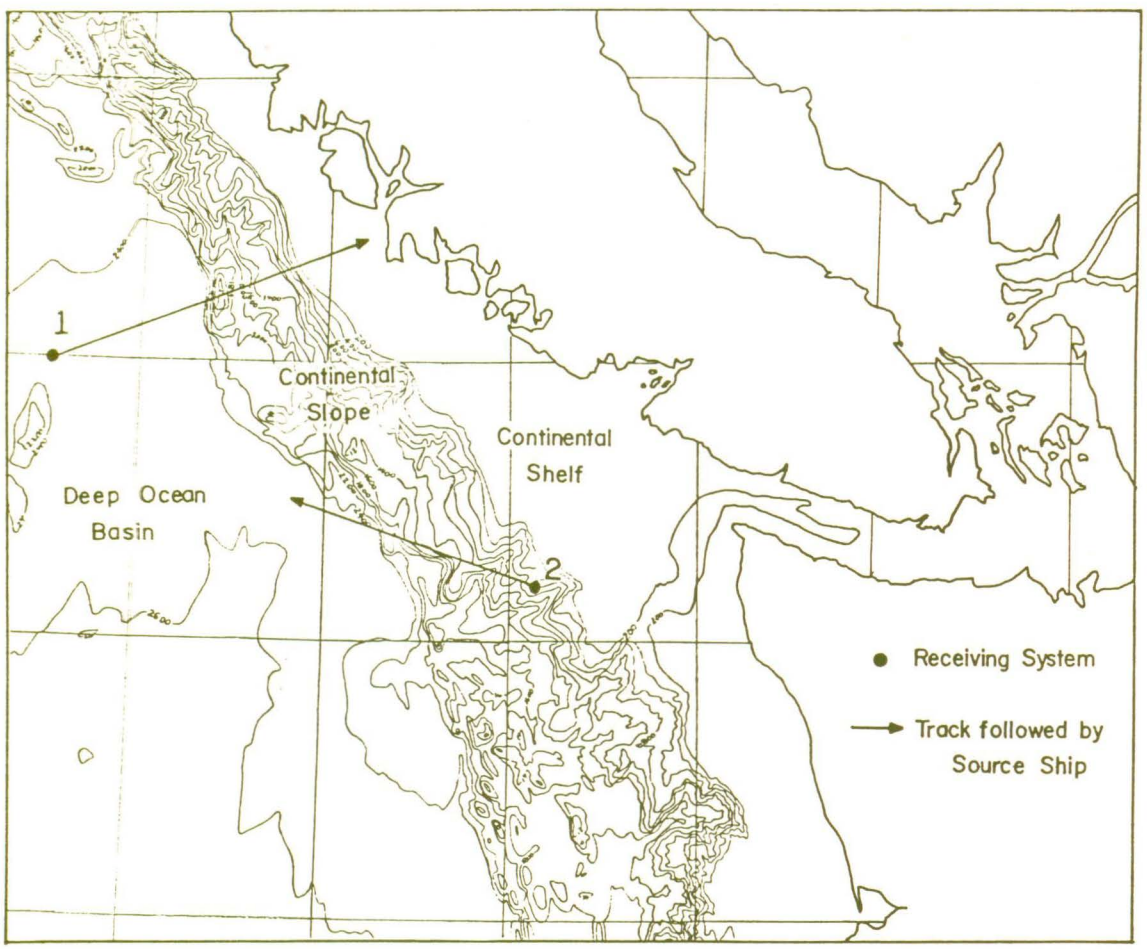


Fig. 2.2. Shot run tracks for the propagation experiment.

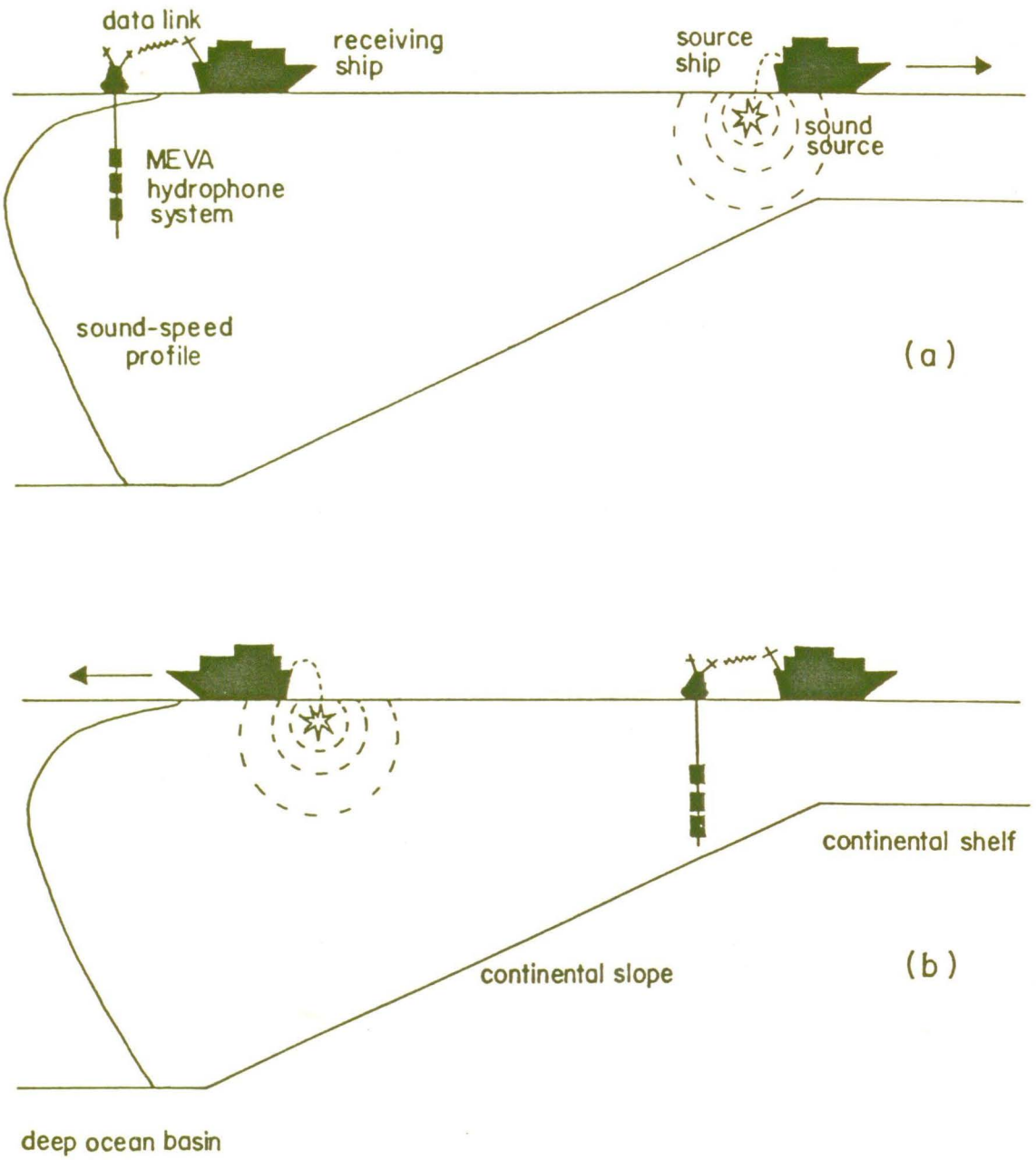


Fig. 2.3. The source-receiver configurations for (a) downslope, and (b) upslope propagation shot runs.

where $P(\omega)$ and $p(t)$ are a Fourier transform pair defined by

$$P(\omega) = F\{p(t)\} = \int_{-\infty}^{\infty} p(t)e^{-i\omega t}dt$$

$$p(t) = F^{-1}\{P(\omega)\} \quad \frac{1}{2\pi}\int_{-\infty}^{\infty} P(\omega)e^{i\omega t}d\omega \quad . \tag{2.3}$$

The contribution due to the ambient noise may be removed to give the acoustic flux density E due to the source alone:

$$E(r) = \frac{1}{2\pi\rho c}\int_{-\infty}^{\infty} (|P(\omega)|^2 - |N(\omega)|^2)d\omega \quad , \tag{2.4}$$

where $N(\omega)$ is the Fourier transform of $n(t)$. This may be averaged into 1/3-octave frequency bands according to

$$E_{1,2}(r) = \frac{1}{2\pi\rho c(\omega_2-\omega_1)}\int_{\omega_1}^{\omega_2} (|P(\omega)|^2 - |N(\omega)|^2)d\omega \quad , \tag{2.5}$$

where $E_{1,2}$ is the acoustic flux density in the frequency band between $\omega_1$ and $\omega_2$ (a 1/3-octave frequency band is a band for which $\omega_2 = 2^{1/3}\omega_1$; the centre frequency of the band is defined to be geometric mean $(\omega_1\omega_2)^{1/2}$). The propagation loss in 1/3-octave bands is defined as

$$H_{1,2}(r) = 10\log\left(\frac{E_{1,2}(1)}{E_{1,2}(r)}\right)$$

$$= 10\log E_{1,2}(1) - 10\log E_{1,2}(r)$$

$$= SL_{1,2} - RL_{1,2} \quad , \tag{2.6}$$

where $SL_{1,2}$ and $RL_{1,2}$ are the energy levels in dB at a distance of 1 m from the source and at the receiver, respectively.

In carrying out the experiment described in Section 2.1, a pressure time series was recorded at the receiving system for each source. This time series consisted of a 5.5 s sample of the ambient noise, n(t), and an 8.2 s record which included all the multipath signal arrivals, p(t). The signal to noise excess was at least 20 dB for all records. The acoustic flux density at the receiver due to the source alone was calculated in 1/3-octave bands from 25 to 630 Hz according to Eq. (2.5) using the discrete fast Fourier transform to calculate the Fourier transforms. The propagation loss was calculated for each source according to Eq. (2.6), making use of this acoustic flux density and source level values $SL_{1,2}$ measured by Chapman (1983a).

The source-receiver ranges were calculated using the recorded source ship and receiving ship locations. These ranges could also be calculated by determining the travel times of the acoustic arrivals and assuming an average sound-speed value. Unfortunately, the travel times could not always be determined due to problems with the reference radio tone transmitted by the source ship to indicate source detonation. Range values that could be calculated by both methods agreed generally to within 1 km.

# CHAPTER 3
# ACOUSTIC PROPAGATION OVER THE CONTINENTAL SLOPE

## 3.1 Downslope Propagation Results

Acoustic propagation in an ocean of varying depth is, in general, a complex process dependent on the depth and sound-speed structure of the ocean, and the geometry and composition of the ocean bottom. The purpose of this chapter is to present the results of the propagation experiments described in Chapter 2, and to interpret these results for the recorded oceanographic environments. In this section the results of the downslope propagation shot run (shot run 1) are described. The results of the upslope propagation shot run (shot run 2) are considered in Section 3.2.

The bathymetry and sound-speed profiles measured along the track of shot run 1 are shown in Fig. 3.1. The ocean floor along the 130-km track includes three distinct bathymetric regions: the deep ocean basin (0-70 km in range), the continental slope (70-110 km in range) and the continental shelf (110-130 km in range). The ocean depth varies from about 2500 m over the ocean basin to about 150 m over the continental shelf. In both these regions the ocean floor is relatively flat and regular. Along the continental slope the ocean floor is more irregular. The pinnacle at 75 km in range probably represents an ocean-floor ridge running parallel to the continental shelf.

A total of five sound-speed profiles were recorded along the shot run track at 25-km range intervals (the ranges at which the profiles were recorded are indicated by the intersection of the profile with the ocean floor). These profiles exhibit a feature common to deep oceans: the deep sound channel. The upper region of negative (downward refracting) gradient is caused by the decrease in sound speed with temperature over the first few hundred metres below the ocean surface; the lower region of positive

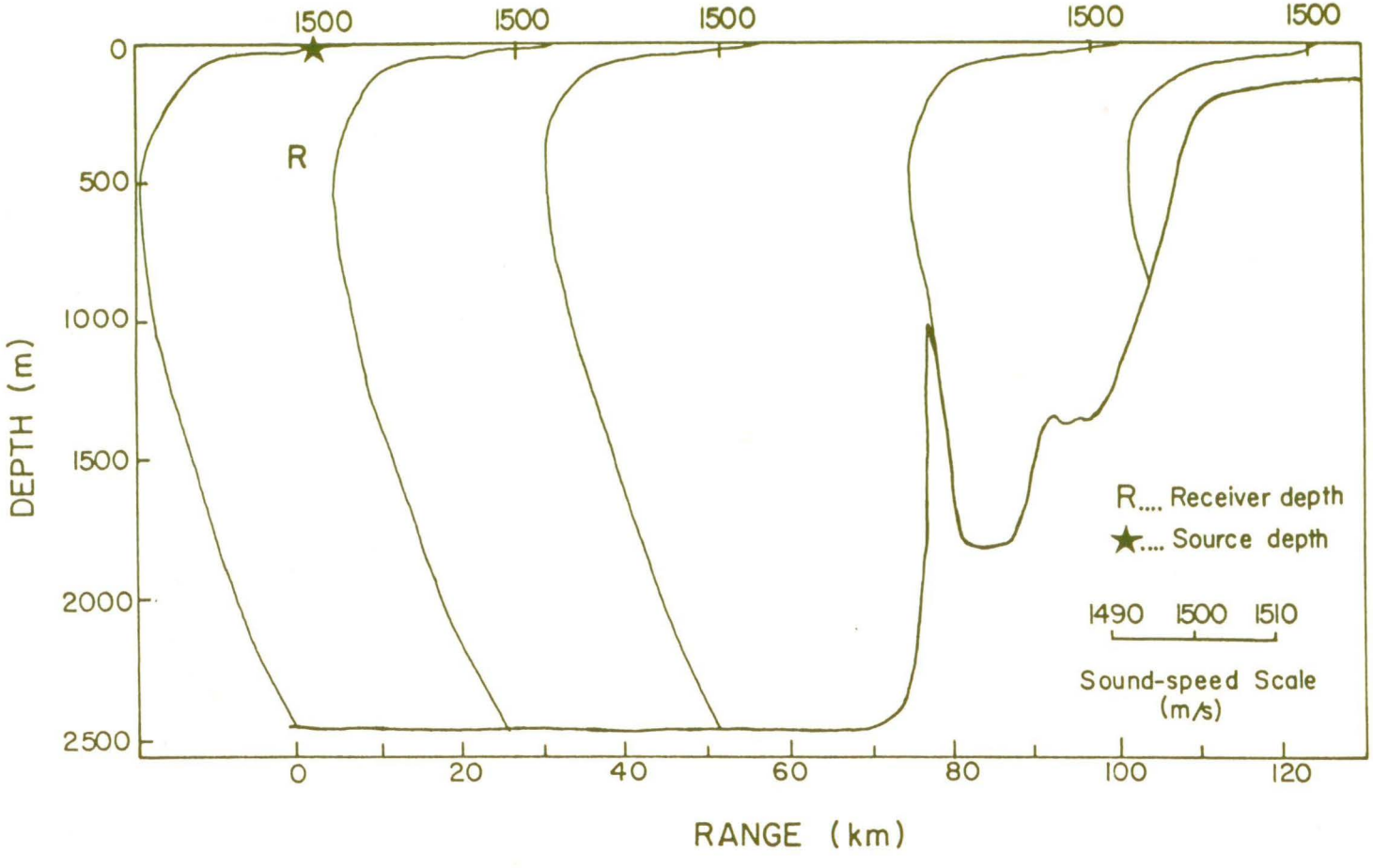


Fig. 3.1. The bathymetry and sound-speed profiles recorded for shot run 1.

(upward refracting) gradient is caused by the increase in sound speed with pressure in the deep isothermal water. The existence of the deep sound channel and its ability to transmit sound to long ranges via continuously refracted propagation paths have been well known since World War II.

The sound-speed minimum, or axis, of the deep sound channel is at a depth of about 400 m. Since this is the optimum depth for detecting sound propagating in the water column, the acoustic pressure measurements recorded at a hydrophone 380 m deep were selected for analysis. The source depth of 22 m is within the steep negative sound-speed gradient and consequently ensures strong acoustic interaction with the ocean bottom.

Figure 3.2 shows the propagation loss with range measured in shot run 1 for the 1/3-octave frequency band centred at 400 Hz. The propagation loss values measured for each source are indicated by closed circles which are connected to delineate trends in these measurements. The ocean-floor bathymetry along the shot run track is shown below the propagation loss curve.

To illustrate the effects of the varying ocean-floor geometry on the acoustic propagation, an estimate of the propagation loss for a 2500 m deep ocean basin with a flat bottom is included in Fig. 3.2 for comparison. This propagation loss curve was calculated by estimating the losses due to geometrical spreading, attenuation and bottom interaction for a range-independent ocean. The loss due to geometrical spreading of the acoustic wavefront was calculated according to (Urick, 1983)

$$H_S(r) = 10\log(r_o r) \quad , \qquad (3.1)$$

where $r_o$ was taken to be 2500 m, equal to the ocean depth. This model approximates spherical spreading loss out to a range equal to the ocean

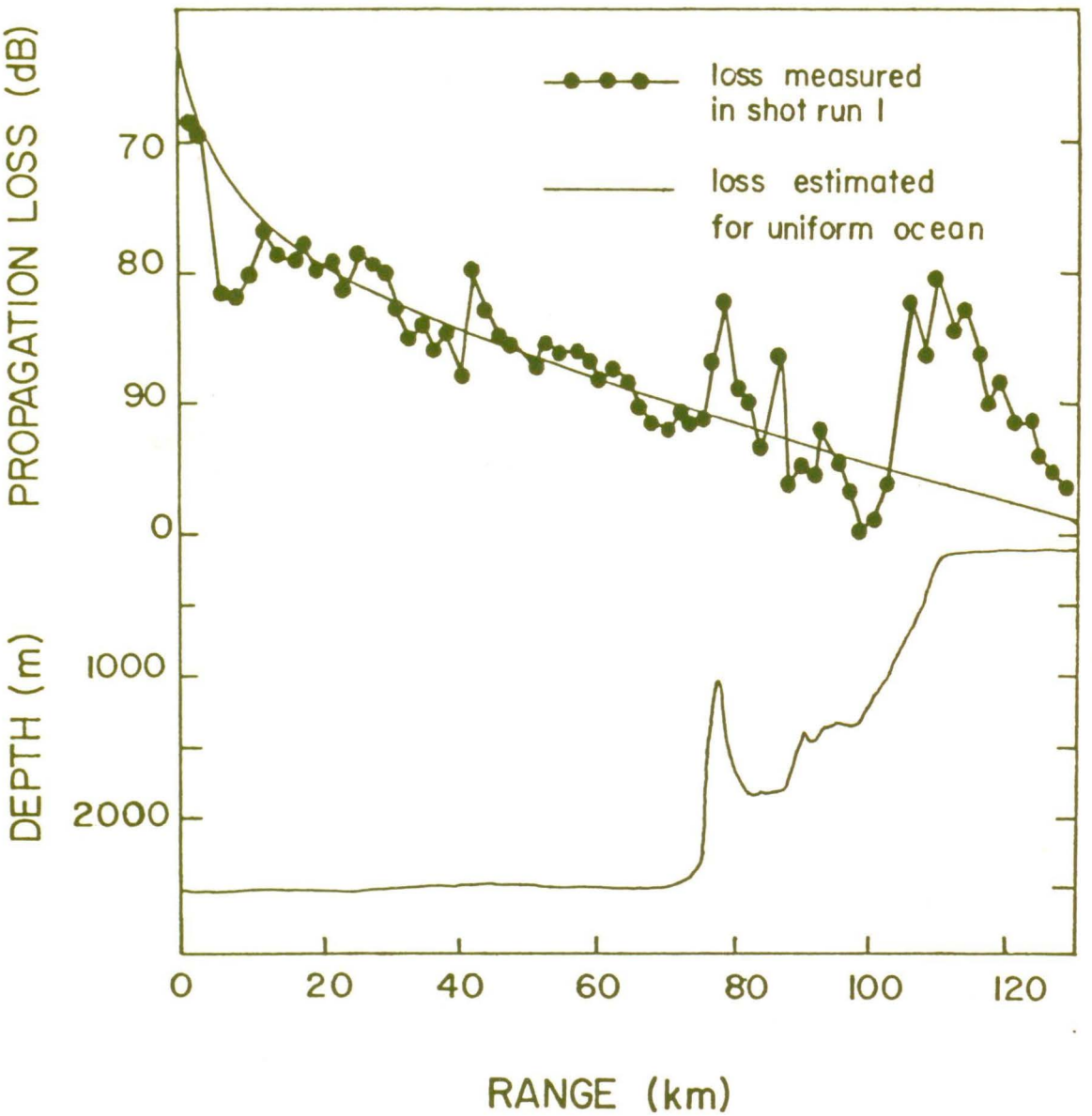


Fig. 3.2. Propagation loss measured in shot run 1 (bathymetry shown) is compared to the estimated loss for 2500-m deep ocean basin with a flat bottom for a frequency of 400 Hz.

depth and cylindrical spreading loss at greater ranges. Attenuation in the water column due to large scale scattering, chemical absorption ($B(OH)_3$ and $MgSO_4$ relaxation processes), and viscosity was calculated according to

$$H_A(r) = \alpha r \quad , \tag{3.2}$$

where $\alpha$ was calculated to be 0.02 dB/km for a frequency of 400 Hz using a semi-empirical expression given by Urick (1982):

$$\alpha(\text{dB/km}) = 0.004 + \frac{0.1f^2}{1 + f^2} + \frac{44f^2}{4100 + f^2} + 0.0003f^2 \quad , \tag{3.3}$$

where f is the frequency in kHz. In order to estimate the bottom loss $\beta$ in dB/km, the propagation loss due to spreading and attenuation calculated according to Eqs. (3.1) - (3.3) was compared to the propagation loss values measured in shot run 1 over the deep ocean basin region (0-70 km in range). The measured loss exceeded the loss calculated for spreading and attenuation at all ranges in this region. The excess loss, estimated to be 0.09 dB/km, was assumed to be due to bottom interaction. Using this value for $\beta$ the bottom loss was calculated as

$$H_B(r) = \beta r \quad . \tag{3.4}$$

The propagation loss estimate for a uniformly deep ocean was taken to be the sum of the spreading, attenuation and bottom losses:

$$H(r) = H_S(r) + H_A(r) + H_B(r) \quad . \tag{3.5}$$

In the deep ocean basin region (0-70 km in range), the measured and estimated propagation losses are in reasonably good agreement, as shown in Fig. 3.2. Small-scale fluctuations (2-3 dB) in the measured values could be due to inconsistent source levels, interference and diffraction effects, and variations in the ocean sound-speed structure and in the bottom roughness and composition. Larger variations in the measured loss at ranges near 5 and 40 km are caused by the focusing of sound in the deep sound channel and will be discussed later. The simple propagation loss estimate expressed by Eq. (3.5) ignores all of these effects and predicts an average propagation loss curve for a uniform ocean environment.

The effects of the varying bottom bathymetry are evident in the continental slope region (70-110 km in range) where the measured propagation loss differs significantly from the loss estimated for a uniformly deep ocean. The measured values decrease abruptly at about 100 to 110 km in range where the sloping bottom is relatively regular and monatonic. A minimum of about 80 dB occurs at 110 km in range, near the edge of the continental shelf. This level is 16 dB less than that estimated for a uniformly deep ocean, and is equivalent to levels measured at ranges of 25-30 km over the deep ocean basin. This effect, known as slope enhancement, was also observed by Northrop et al. (1968) in a long-range propagation experiment off the coast of California. A similar but smaller enhancement effect occurs over the ocean-bottom ridge at 75 km in range.

In the continental shelf region (110-130 km in range) the measured propagation loss increases rapidly with range from the enhanced level recorded at the shelf edge. The rate of increase is considerably greater than that predicted for a uniformly deep ocean basin.

It is apparent from Fig. 3.2 that the ocean-floor bathymetry is an important factor influencing the acoustic propagation in this shot run.

The measured propagation loss curve behaves differently in each of the three bathymetric regions. To understand the acoustic propagation in each region, it is useful to consider the propagation paths involved. Some of the paths are shown for each region in Fig. 3.3, where acoustic rays (normals to the propagating wavefronts) have been traced out using the numerical ray model GRASS (Cornyn, 1973a; Cornyn, 1973b; Hoffman and Thomson, 1978). The ray paths were calculated for the ocean environment of Fig. 3.1 by applying Snell's law assuming specular reflection at the ocean boundaries. For clarity and simplicity, only rays which leave the source at shallow angles (within $\pm 10^0$ with respect to the horizontal) are shown. The purpose of this figure is to demonstrate the different propagation paths in each region: no inference of intensity should be made from the ray densities. It should be noted that, in keeping with the convention for ray tracings, the range axes are reversed in Fig. 3.3.

In Fig. 3.3(a) propagation paths are traced out for a 22-m deep source at a range of 70 km in the deep ocean basin region. The strong negative sound-speed gradient near the surface refracts the acoustic rays downward to the ocean floor. Propagation is almost entirely along paths involving two or more bottom reflections over the 70-km range. Rays which leave the source at angles steeper than $\pm 10^0$ interact with the bottom more frequently and at steeper angles than those shown. Bottom interactions, particularly at steep angles, are generally quite lossy, and propagation loss is high for paths involving multiple reflections. Only rays which leave the source at very shallow angles propagate in the deep sound channel without interacting with the ocean bottom, as shown by the $0^0$ (at the source) ray which cycles near the bottom at about 50 km in range.

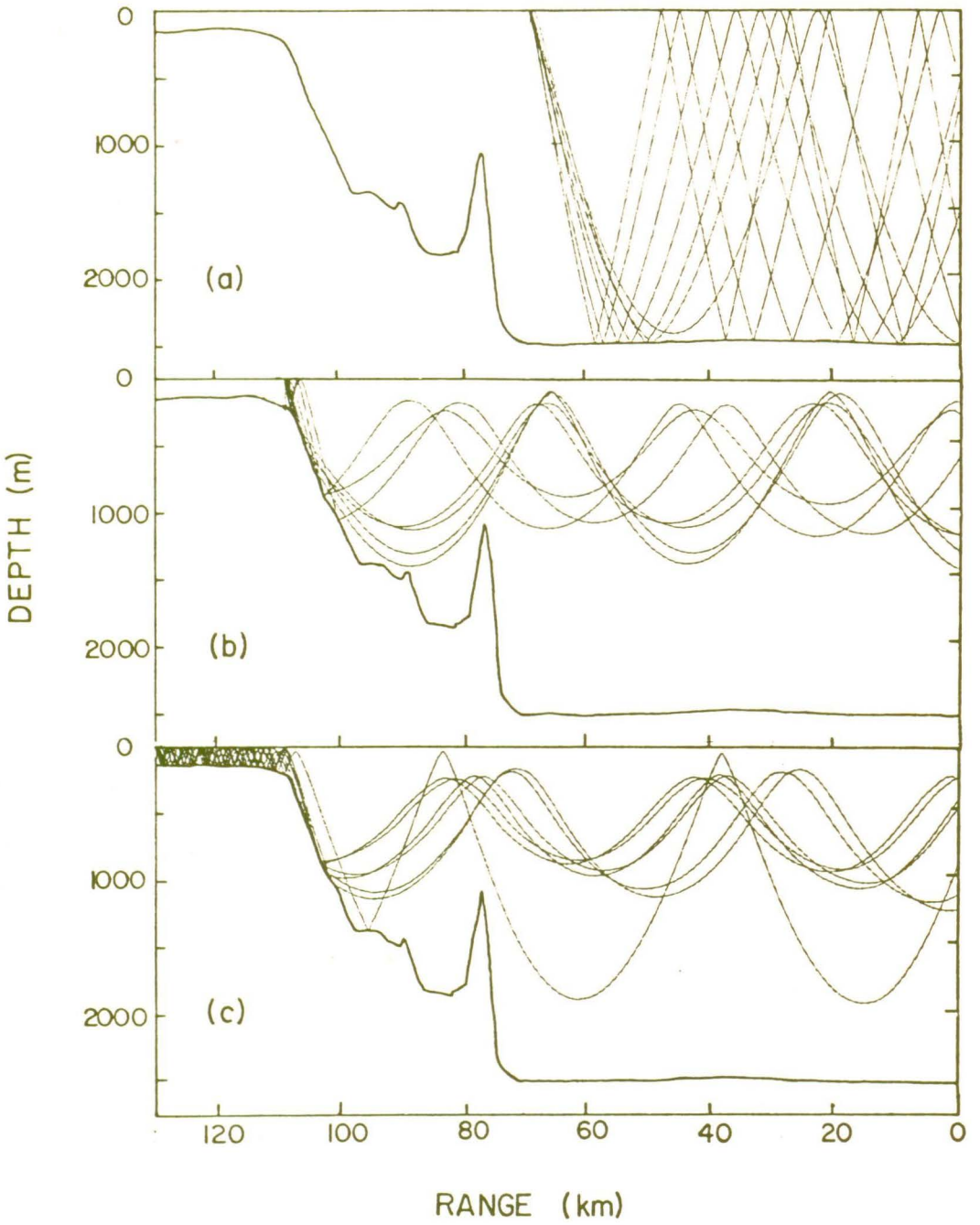


Fig. 3.3. Propagation paths predicted by the numerical ray model GRASS for 22-m deep sources at ranges of (a) 70 km, (b) 110 km, and (c) 130 km for source angles within $\pm 10^0$ (with respect to the horizontal).

The deviations in the measured propagation loss at ranges near 5 and 40 km, shown in Figure 3.2, are commonly observed for the source and receiver depths used in the experiment, and may be explained in terms of ray theory. At about 5-10 km in range the receiver is in an acoustic shadow: the acoustic rays from the source are refracted below the receiver and any bottom-reflected rays arriving at the receiver incur large losses at the bottom due to the steep angles of incidence for such short ranges. This results in a slightly greater propagation loss than that at longer or shorter ranges. The local minimum in loss at about 40 km in range is caused by the acoustic rays which cycle in the deep sound channel without interacting with the ocean bottom are refracted upward to the receiver. The cycle distance from the source to a receiver 380 m deep is about 40 km.

The propagation paths traced out for a source in the continental slope region at a range of 110 km demonstrate entirely different propagation paths, as shown by Fig. 3.3(b). As the acoustic rays propagate down the continental slope, each bottom reflection reduces the ray angle by twice the slope angle. One or more bottom reflections may reduce the angle sufficiently for the ray to become continuously refracted within the deep sound channel and propagate without further bottom interactions. Sound propagating in the sound channel suffers only cylindrical spreading and attenuation losses and is not subject to the losses associated with repeated bottom interactions. In addition, the conversion from spherical spreading to cylindrical spreading at a shallower depth results in less spreading loss. Assuming a conversion from spherical to cylindrical spreading at a depth of 500 m and negligible bottom losses, the propagation loss for a source at 110 km in range according to Eq. (3.5) is 79.5 dB, about 0.5 dB less than the value measured at that range. By this downslope conversion to low loss paths, a receiver in the deep sound channel may measure greater intensity for a distant source located over a sloping ocean bottom than for a nearer source located over a flat bottom. This

accounts for the slope enhancement effect at 100-110 km in range in Fig. 3.2. Ray tracings for a source over the ocean-floor ridge (not shown) indicate that the decrease in propagation loss at 75-80 km in range, shown in Fig. 3.2, is also a slope-enhancement effect. The uneven ocean floor between about 80 and 100 km in range accounts for the large variations in loss measurements at these ranges.

Figure 3.3(c) shows the acoustic ray paths traced out for a source in the continental shelf region at a range of 130 km. The rays are refracted downward by the negative sound-speed gradient near the surface and interact repeatedly with the ocean bottom in the shallow waters over the shelf before propagating into deeper waters. The rapid increase in propagation loss with range in the continental slope region, shown in Fig. 3.2, is caused by the high rate of loss due to bottom interactions in this region.

The acoustic ray tracings of Fig. 3.3 show different propagation paths for sources in each of the three bathymetric regions. These differences are also apparent in the sequence of arrivals and the frequency content of the pressure time series, or pressure histories, recorded for sources in each region. Figures 3.4 - 3.6 show the pressure histories, broadband in frequency and filtered into 50-Hz passbands centred at 50, 250, and 500 Hz, recorded for the three source locations used in the ray tracings of Fig. 3.3.

Figure 3.4 shows 4.5 s of the pressure history for the source at 70-km range in the deep ocean basin region. Zero time is defined as the time of the first detectable signal. The 50-Hz passbands are normalized to correct for variations in the source level with frequency. The five distinct arrivals evident in the broadband pressure history can be identified as bottom-reflected arrivals by their characteristic four-path

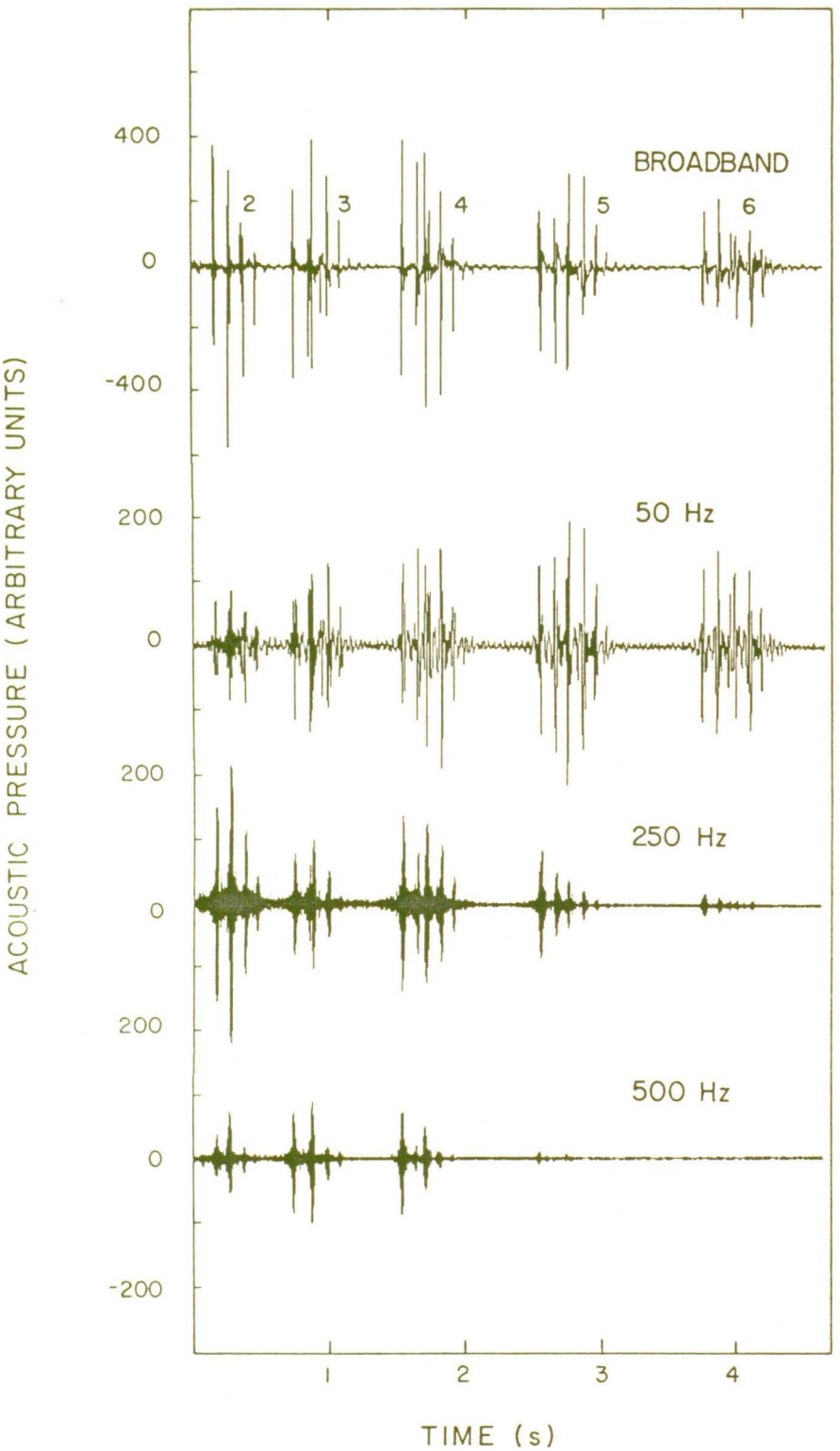


Fig. 3.4. Pressure history, broadband and in 50 Hz passbands centred at 50, 250 and 500 Hz, recorded for the source at 70 km in range in the deep ocean basin region.

structure (including phase reversals due to surface reflections) typical for the source and receiver depths used in the experiment. Examination of the pressure histories recorded for shorter ranges identifies the five arrivals as those involving two, three, four, five and six bottom reflections (the number of bottom reflections is indicated for each arrival on the broadband pressure history). This agrees with the ray analysis of Fig. 3.3(a) which predicts no direct or single bottom-reflection propagation paths from source to receiver.

The three 50-Hz passbands in Fig. 3.4 show that the amplitude of the five arrivals generally decreases with increasing frequency, and that this decrease is most pronounced for the arrivals involving the most bottom interactions. For example, although the arrivals involving 5 and 6 bottom interactions have large amplitudes at 50 Hz, at 500 Hz they are almost undetectable. This behavior, which is typical for propagation paths involving multiple interactions with a penetrable ocean bottom (Christensen et al., 1974), can be explained by considering the bottom loss mechanisms which include scattering and transmission into the ocean bottom sediment layers. Losses due to scattering at the ocean floor generally increase with frequency. Sound which enters the sediments may be reflected back into the water column by sub-bottom layers or refracted back by the steep sound-speed gradient. Attenuation along such sub-bottom paths also increases with frequency (Hamilton, 1980, reports a first power dependence on frequency). As seen in Fig. 3.4 this frequency dependence is most pronounced for arrivals which have suffered numerous bottom interactions, since the losses are cumulative and the interactions occur at steeper angles which result in greater transmission into the sediments. The frequency content of the arrivals can be used to help identify the propagation paths involved (Vidmar, 1982).

Figure 3.5 shows the pressure history recorded for a source in the continental slope region at range of 110 km, where the slope enhancement effect is a maximum. The sequence of arrivals is quite different from that for a source over the deep ocean basin: instead of a series of distinct bottom-reflected arrivals, one very strong arrival was recorded. The structure of this arrival indicates that it involves a number of different propagation paths. These observations are consistent with the ray analysis of Fig. 3.3(b). Acoustic rays which interact one or even two times with the ocean bottom at different ranges along the continental slope before entering the deep sound channel do not differ greatly in travel time, and could result in the strong initial arrival. The 50 Hz passbands show that the amplitude of the initial arrival decreases with frequency. However, the relatively large amplitude in the 250 and 500 Hz passbands indicate that a major component of the arrival is due to predominantly waterborne propagation paths involving only one or two bottom interactions.

The pressure history recorded for a source at 130-km range in the continental shelf region is shown in Fig. 3.6. The broadband pressure history shows a typical shallow water arrival: a dispersed signal with no sharp pulses or discernable structure. The three 50-Hz passbands show a strong frequency dependence. The relatively small amplitude in the 500-Hz passband indicates numerous bottom interactions. This agrees with the ray analysis of Fig. 3.3(c) which predicts 20 km of strongly bottom-interacting shallow water propagation before the rays enter the sound channel and propagate to the receiver.

To demonstrate the frequency dependence of the different propagation paths for the three bathymetric regions, propagation loss is plotted as a function of frequency for the 70, 110 and 130 km sources in Fig. 3.7. The fluctuations in the measured losses at low frequencies are due to interference effects; these effects are averaged out in the wider

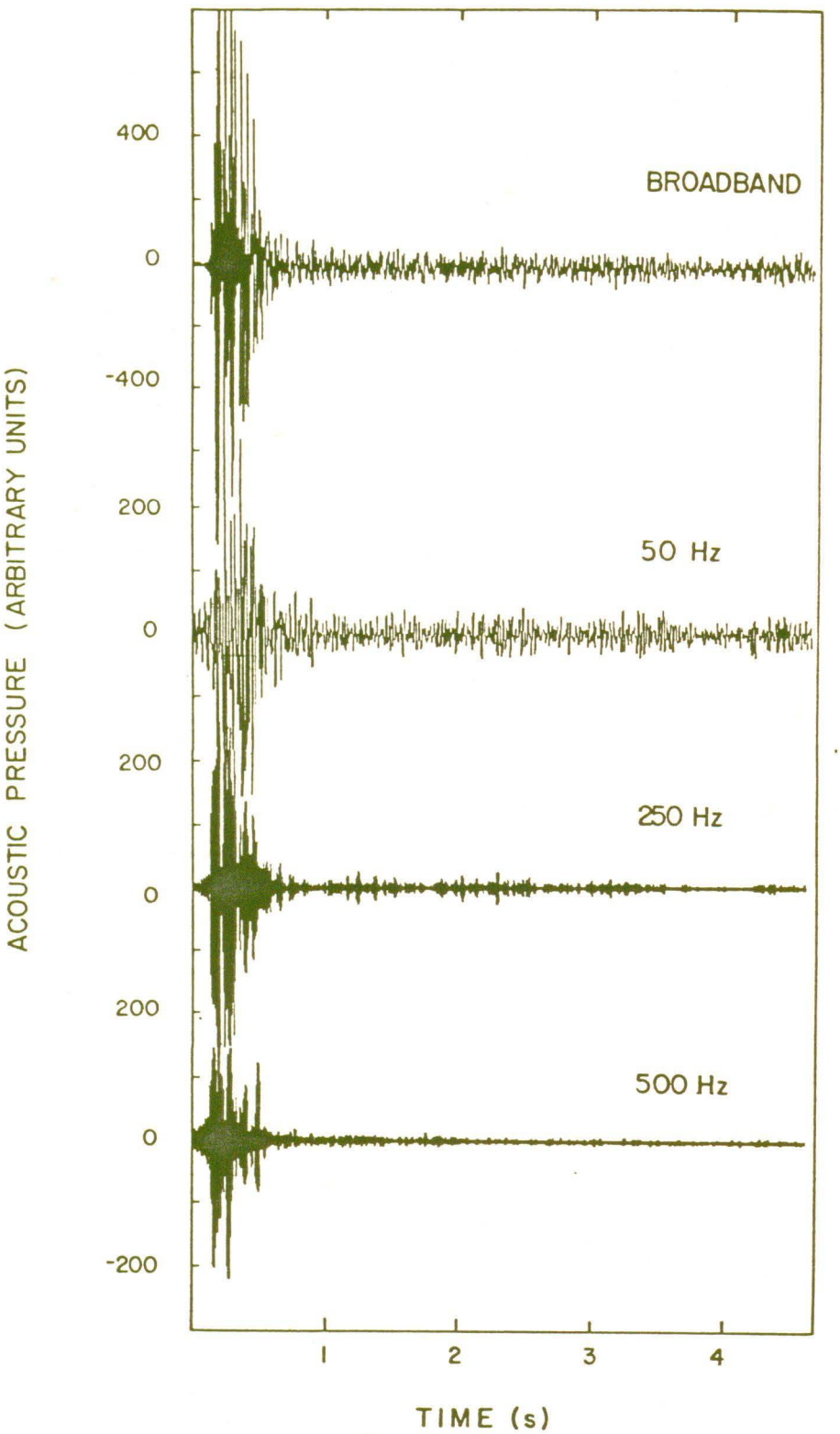


Fig. 3.5 Pressure history, broadband and in 50 Hz passbands centred at 50, 250 and 500 Hz, recorded for the source at 110 km in range tn the continental slope region.

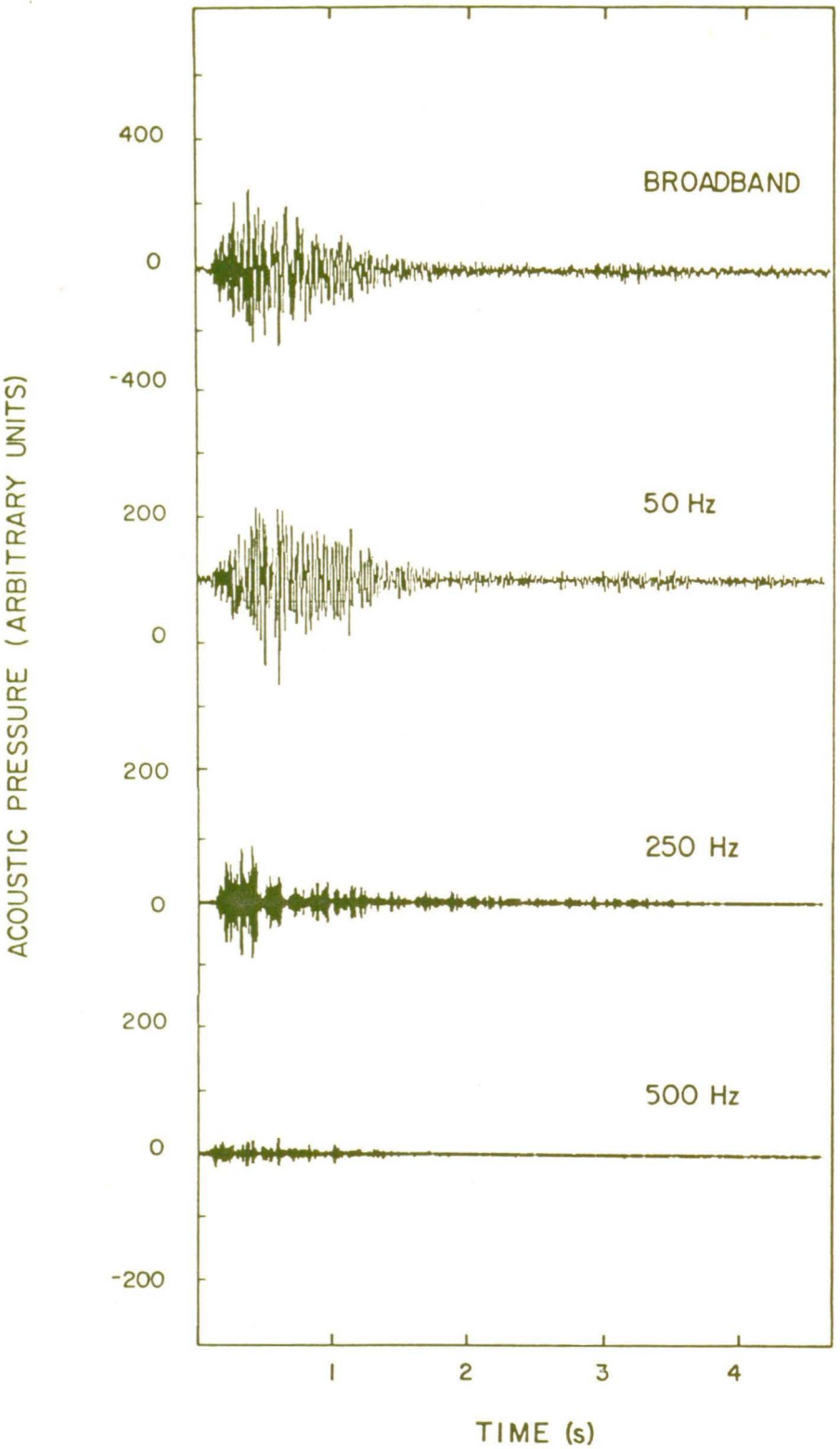


Fig. 3.6 Pressure history, broadband and in 50 Hz passbands centred at 50, 250 and 500 Hz, recorded for the source at 130 km in range in the continental shelf region.

1/3-octave bands at higher frequencies. The different frequency dependence for each source is due to the different propagation paths for each bathymetric region. At low frequencies, where losses due to bottom interactions are quite small, the propagation loss measurements are within about 5 dB. At higher frequencies, where bottom-interaction losses are larger, the propagation loss measurements differ considerably. The least propagation loss at all frequencies was measured for the 110-km (continental slope) source. The loss for this source increases only gradually with frequency indicating minimal bottom-interaction and predominantly waterborne propagation. The propagation loss measured for the 70-km (deep ocean basin) source depends more strongly on frequency indicating bottom-limited acoustic propagation. The greatest loss at all frequencies was measured for the 130-km (continental shelf) source. The rapid increase in loss with frequency is consistent with strongly bottom-interacting propagation in shallow water.

The frequency dependences shown in Fig. 3.7 suggest that the slope enhancement effect is greater at high frequencies than at low frequencies. To demonstrate this, the measured propagation loss is plotted as a function of range in Fig. 3.8 for 1/3-octave frequency bands centred at 25, 200, 400 and 630 Hz. The slope enhancement effects at 75 and 110 km in range are evident at all frequencies, but appear most pronounced at 400 and 630 Hz. This observation can easily be understood. The propagation loss measured over the deep ocean basin, the uneven section of the continental slope region, and the continental shelf increases with frequency due to large bottom-interaction losses. However, the propagation loss measured over the regular sections of the continental slope region remains nearly constant with frequency due to the conversion of bottom-interacting propagation paths into continuously refracted paths. Consequently, the difference in loss levels is greatest at the high frequencies.

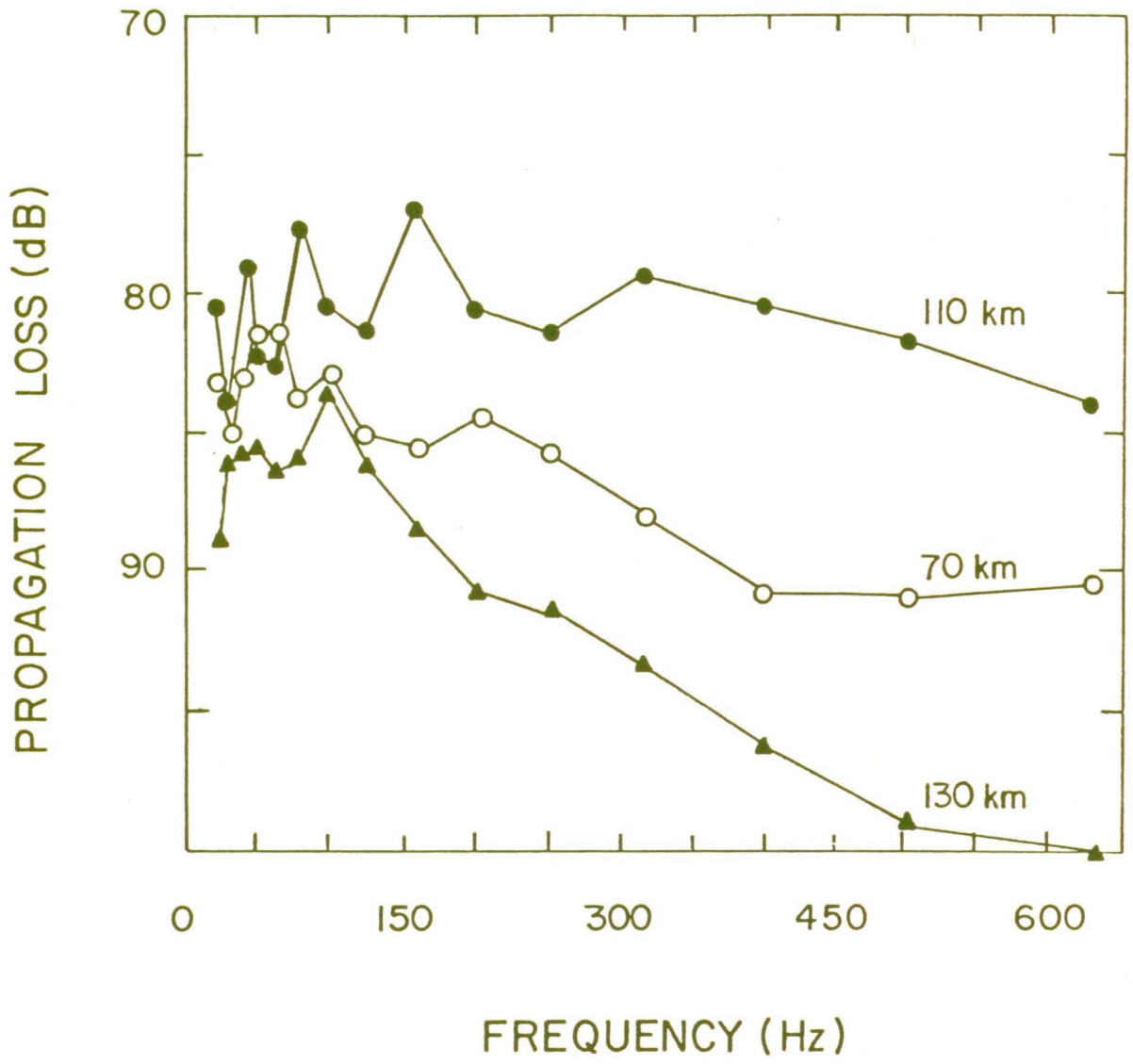


Fig. 3.7 Propagation loss as a function of frequency for sources at 70, 110 and 130 km in range.

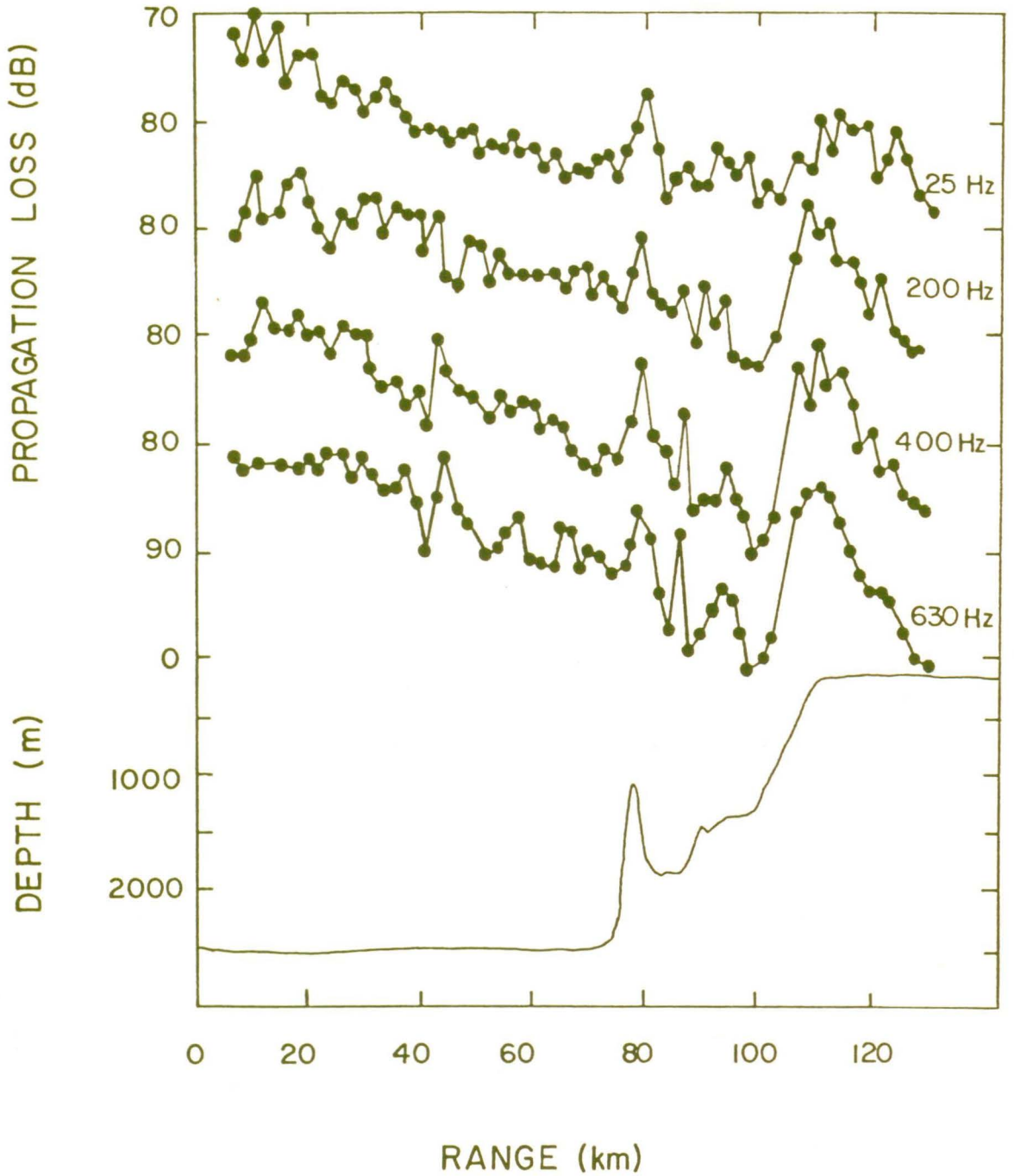


Fig. 3.8. Propagation loss as a function of range (bathymetry shown) for selected 1/3-octave frequency bands centred at 25, 200, 400 and 630 Hz.

## 3.2 Upslope Propagation Results

The bathymetry and sound-speed profiles measured along the track of the upslope propagation shot run (shot run 2) are shown in Fig. 3.9. The ocean floor along the 95-km track consists of two distinct bathymetric regions: the continental slope (0-55 km in range) and the deep ocean basin (55-95 km in range). In the continental slope region the ocean depth varies from about 600 m at the receiver to about 2500 m at the edge of the ocean basin. The ocean floor in this region is quite rough and irregular. In the deep ocean basin region the ocean depth is about 2500 m and the ocean floor is relatively flat and regular. The five sound-speed profiles measured along the track exhibit minima between 400-500 m in depth. The acoustic pressure measurements recorded at a hydrophone near this depth (560 m) were selected for analysis. The shallow source depth (22 m) ensures strong acoustic interaction with the ocean bottom.

The propagation loss values measured in shot run 2 are plotted as a function of range in Fig. 3.10 for the 1/3-octave frequency band centred at 630 Hz. An estimate of the propagation loss for a 2500 m deep ocean basin is included for comparison. This propagation loss curve was calculated by estimating the losses due to geometrical spreading, attenuation and bottom interaction according to Eqs. (3.1) - (3.5). The loss due to bottom interaction was estimated to be 0.10 dB/km from the 630 Hz propagation loss measurements in the deep ocean basin region of shot run 1. Although the bottom losses may differ between the two shot run tracks, this estimate should be adequate for qualitative comparisons.

The propagation loss measured in shot run 2 exceeds that estimated for a uniformly deep ocean at all ranges, as shown in Fig. 3.10. At short ranges the difference is not great, however the measured loss increases rapidly with range in the continental slope region, and exceeds the loss

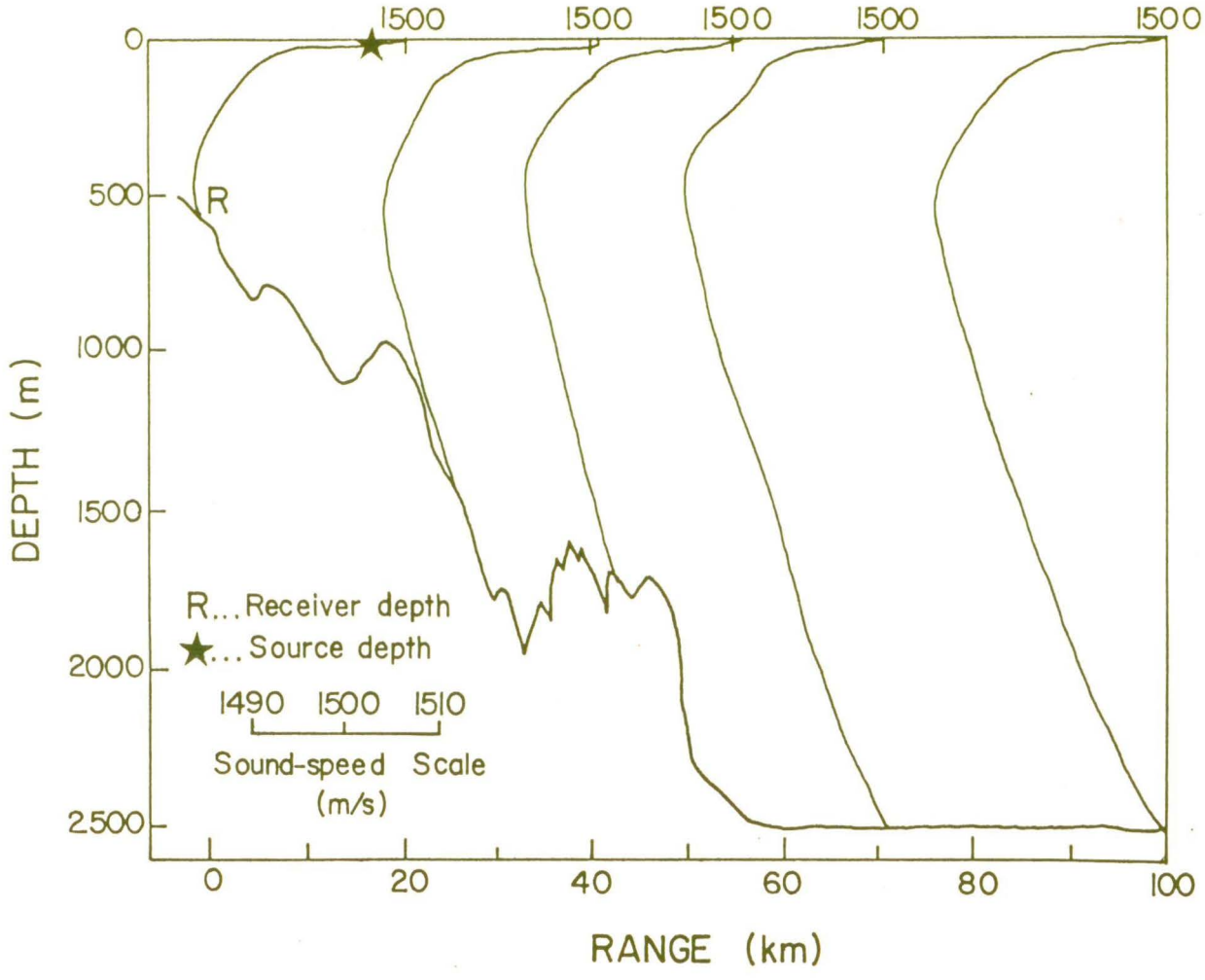


Fig. 3.9. Bathymetry and sound-speed profiles recorded for shot run 2.

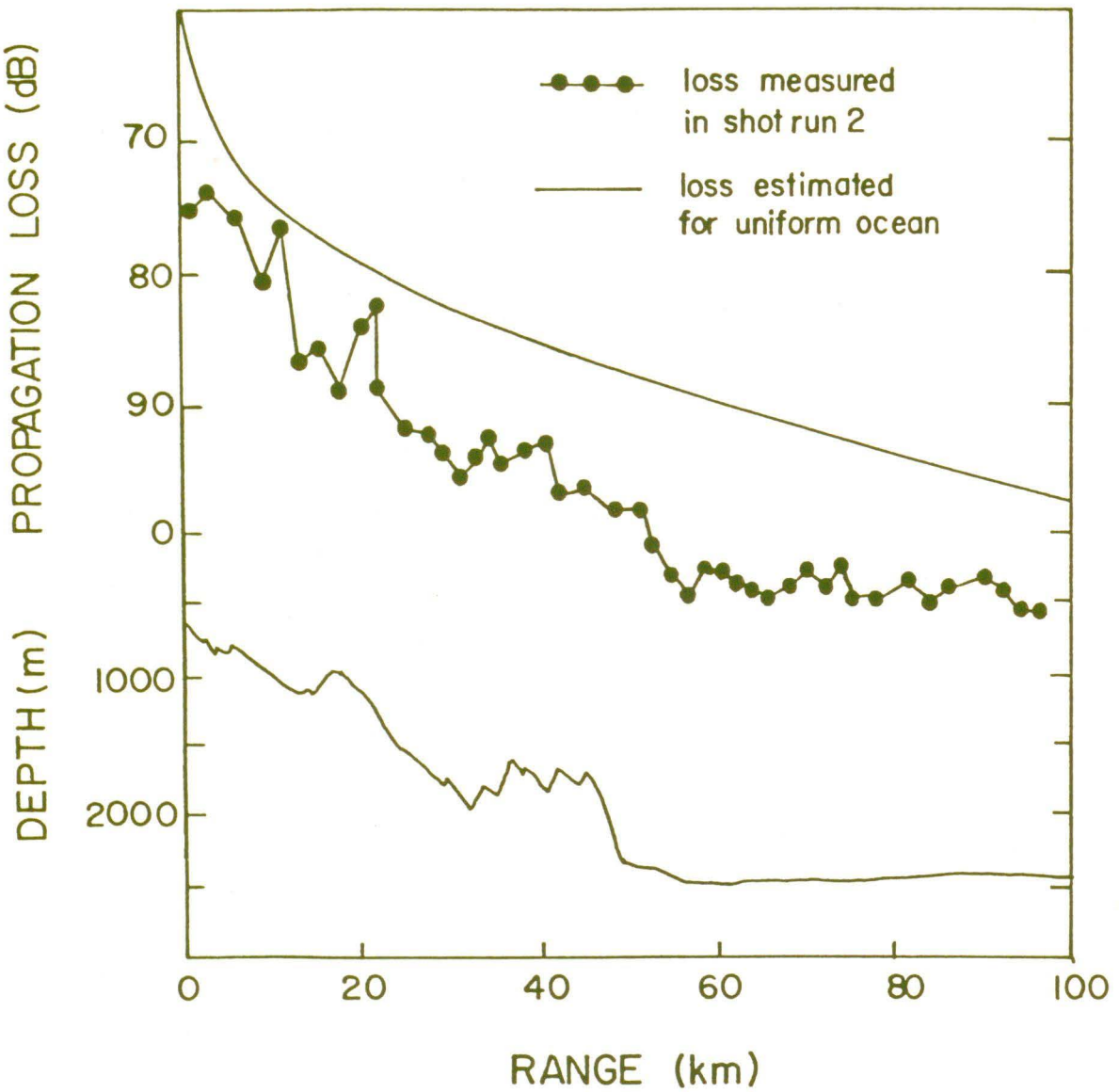


Fig. 3.10. Propagation loss measured in shot run 2 (bathymetry shown) is compared to the estimated loss for a 2500-m deep ocean basin with a flat bottom for a frequency of 630 Hz.

estimated for a uniform ocean by about 15 dB at a range of 55 km. In the deep ocean basin region the measured propagation loss increases more gradually with range than the uniform-ocean estimate, so that at a range of 95 km the measured loss exceeds the estimated loss by only about 9 dB.

It is apparent from the measurements shown in Fig. 3.10 that the acoustic propagation is influenced significantly by the ocean floor bathymetry in the two regions of shot run 2. To illustrate the different propagation paths in each region, Fig. 3.11 shows the acoustic ray paths traced out using the numerical ray model GRASS. For clarity, only the $0^0$ (at the source) ray is shown. Rays which leave the source at steep angles will suffer very high losses in the continental slope region and need not be considered.

Figure 3.11(a) traces the path of an acoustic ray from a 22-m deep source at a range of 55 km in the continental slope region. The strong negative sound-speed gradient near the ocean surface refracts the sound to the ocean floor and the ray propagates up the continental slope by a series of bottom and surface reflections. Each bottom reflection increases the ray angle by twice the angle of the slope. As the ray path steepens, the rate of bottom interactions and the loss per interaction (due to penetration into the ocean bottom) generally increases, resulting in large losses due to bottom interaction in the continental slope region. Since the track of shot run 2 was not perpendicular to the contours of the slope, as shown in Fig. 2.2, additional loss in this region could result from the curvature of ray paths out of the plane of propagation, as described by Harrison (1977), an effect which cannot be modelled by two dimensional ray theory. These mechanisms result in the rapid increase in the propagation loss in the continental slope region shown in Fig. 3.10.

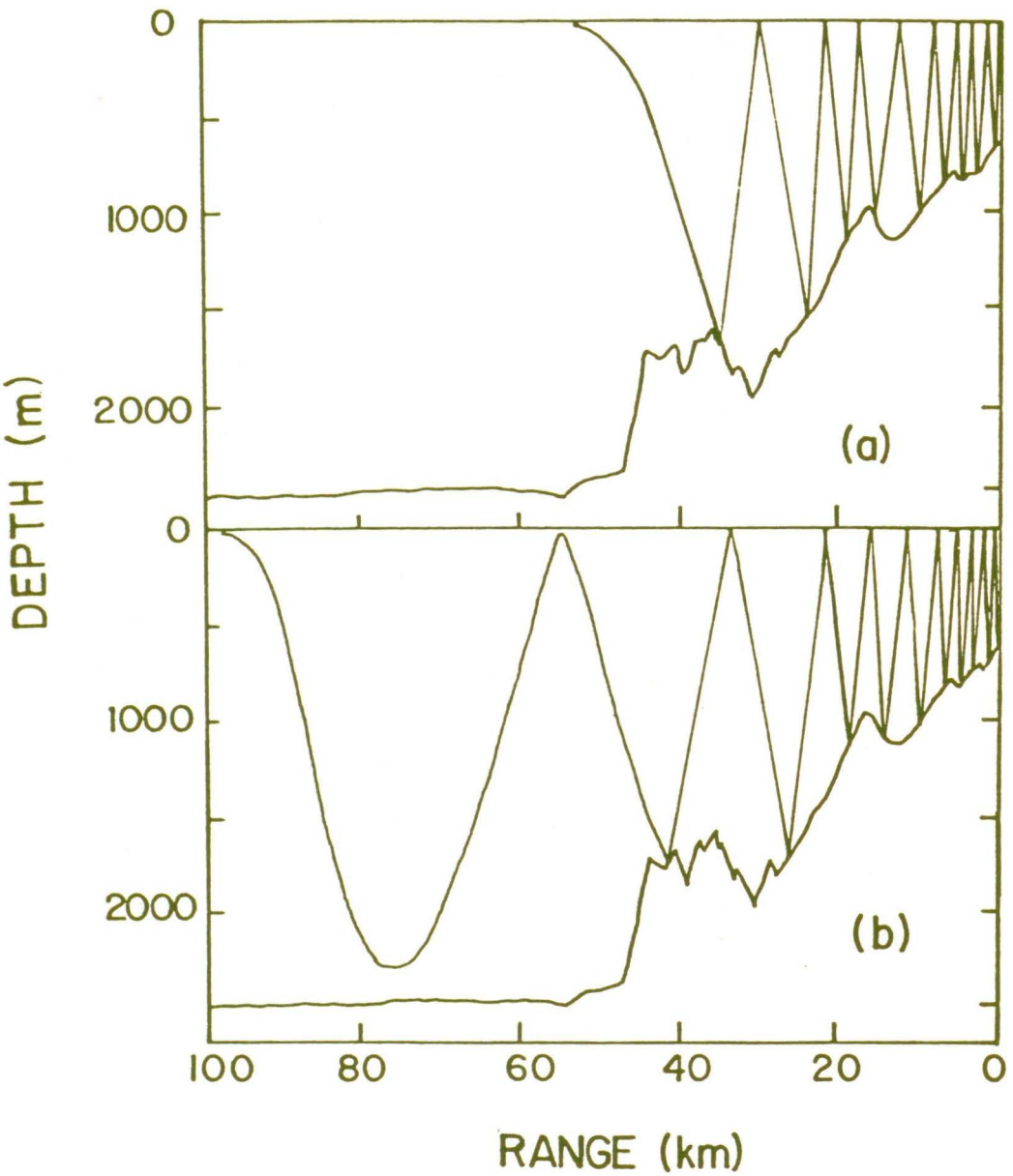


Fig. 3.11. Propagation paths predicted by the numerical ray model GRASS for 22-m deep sources at ranges of (a) 55km, and (b) 95 km for a source angle of 0°.

In Fig. 3.11(b) the propagation path of the $0^0$ source-angle ray is traced out for a source at a range of 95 km in the deep ocean basin region. The ray cycles in the deep sound channel without interacting with the bottom in the ocean basin region before propagating up the continental slope by a series of increasingly steep bottom reflections. Sound propagating within the channel in the deep ocean basin region suffers very little loss compared to the strongly bottom-interacting propagation over the continental slope. Thus the propagation loss values measured for sources in the deep ocean basin region increase only gradually with range, as shown in Fig. 3.10. The relatively large fluctuations in the measured propagation loss values for sources in both regions may be attributed to the irregular bathymetry and variable bottom slopes in the continental slope region.

The pressure histories recorded for the 55-km (continental slope) and 95-km (deep ocean basin) sources are shown in Fig. 3.12 and 3.13, respectively. Although the amplitude is smaller for the source at 95 km in range, the pressure histories and frequency content are very similar for both sources. In each case the broadband pressure history shows a dispersed signal composed of many weak arrivals. The signal amplitude decreases strongly with frequency in the 50-Hz passbands. To demonstrate the frequency dependence, propagation loss is plotted as a function of frequency for the two sources in Fig. 3.14. Although the propagation loss for the source at 95 km in range exceeds that for the source at 55 km in range at all frequencies, the frequency dependence is essentially the same for both sources. The increase in propagation loss with frequency indicates significant losses due to bottom interaction. These observations are consistent with the ray analysis of Fig. 3.11, which predicts strong bottom interaction only in the continental slope region.

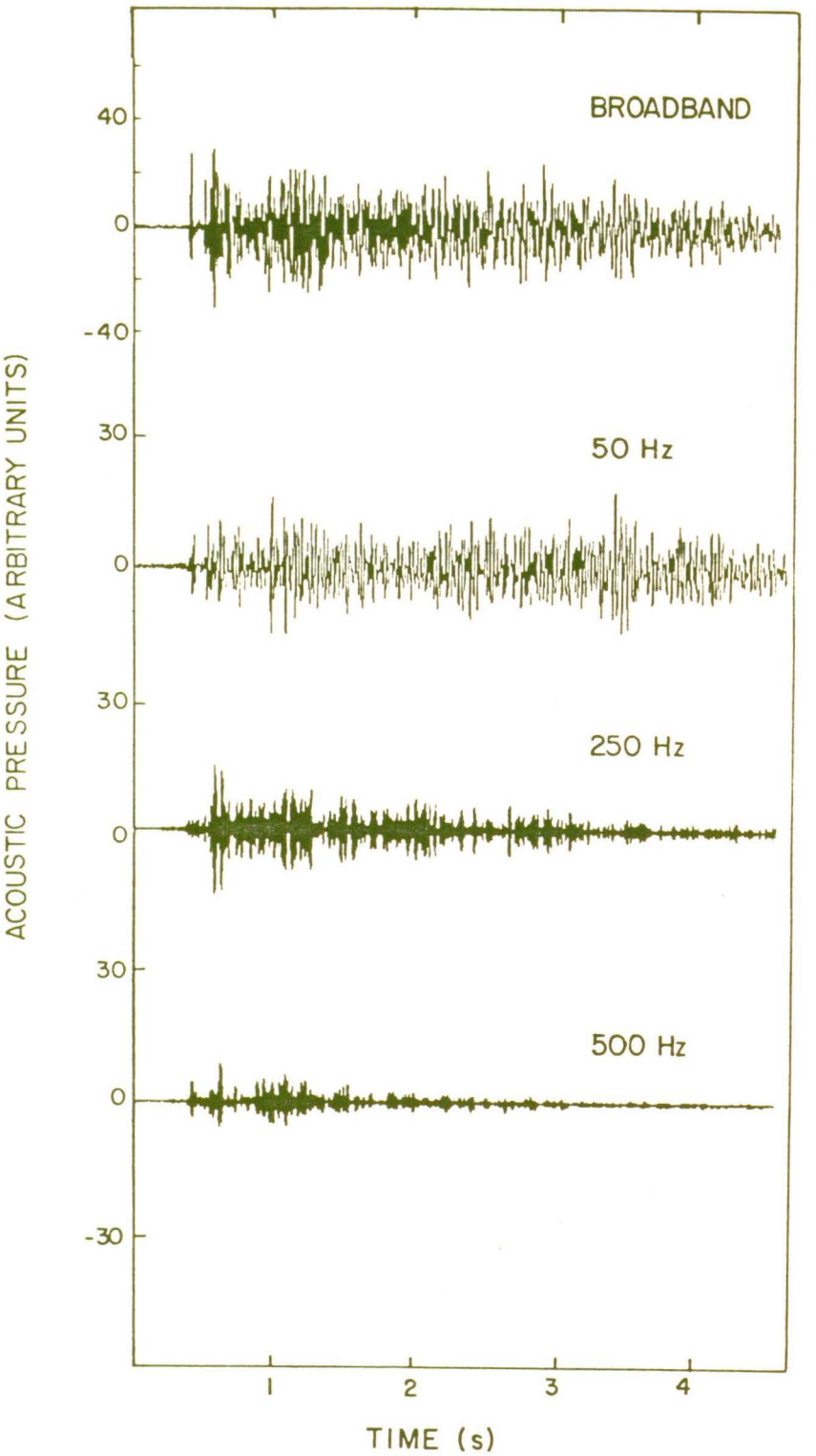


Fig. 3.12. Pressure history, broadband and in 50 Hz passbands centred at 50, 250 and 500 Hz, recorded for the source at 55 km in range in the continental slope region.

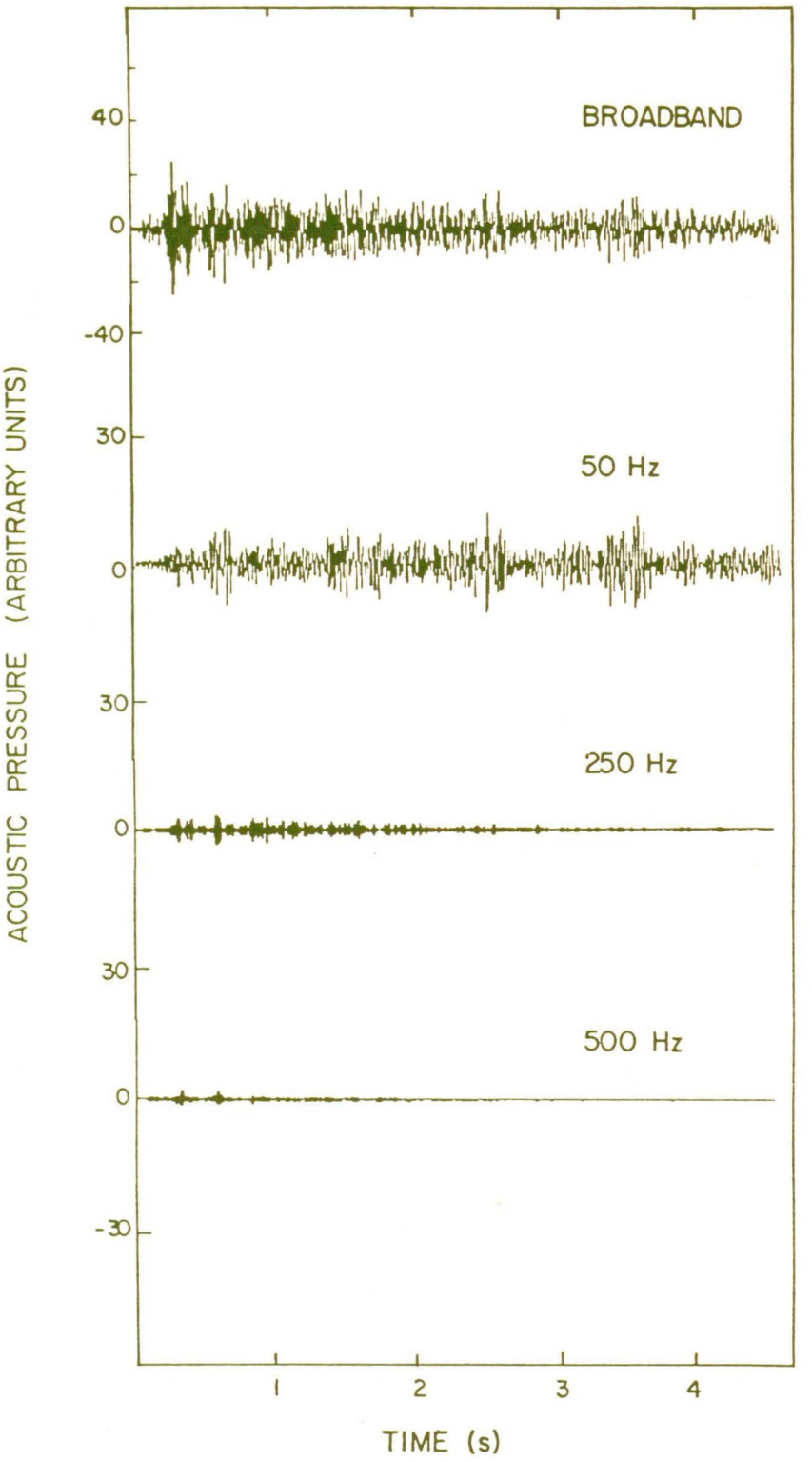


Fig. 3.13. Pressure history, broadband and in 50-Hz passbands centred at 50, 250 and 500 Hz, recorded for the source at 95 km in range in the deep ocean basin region.

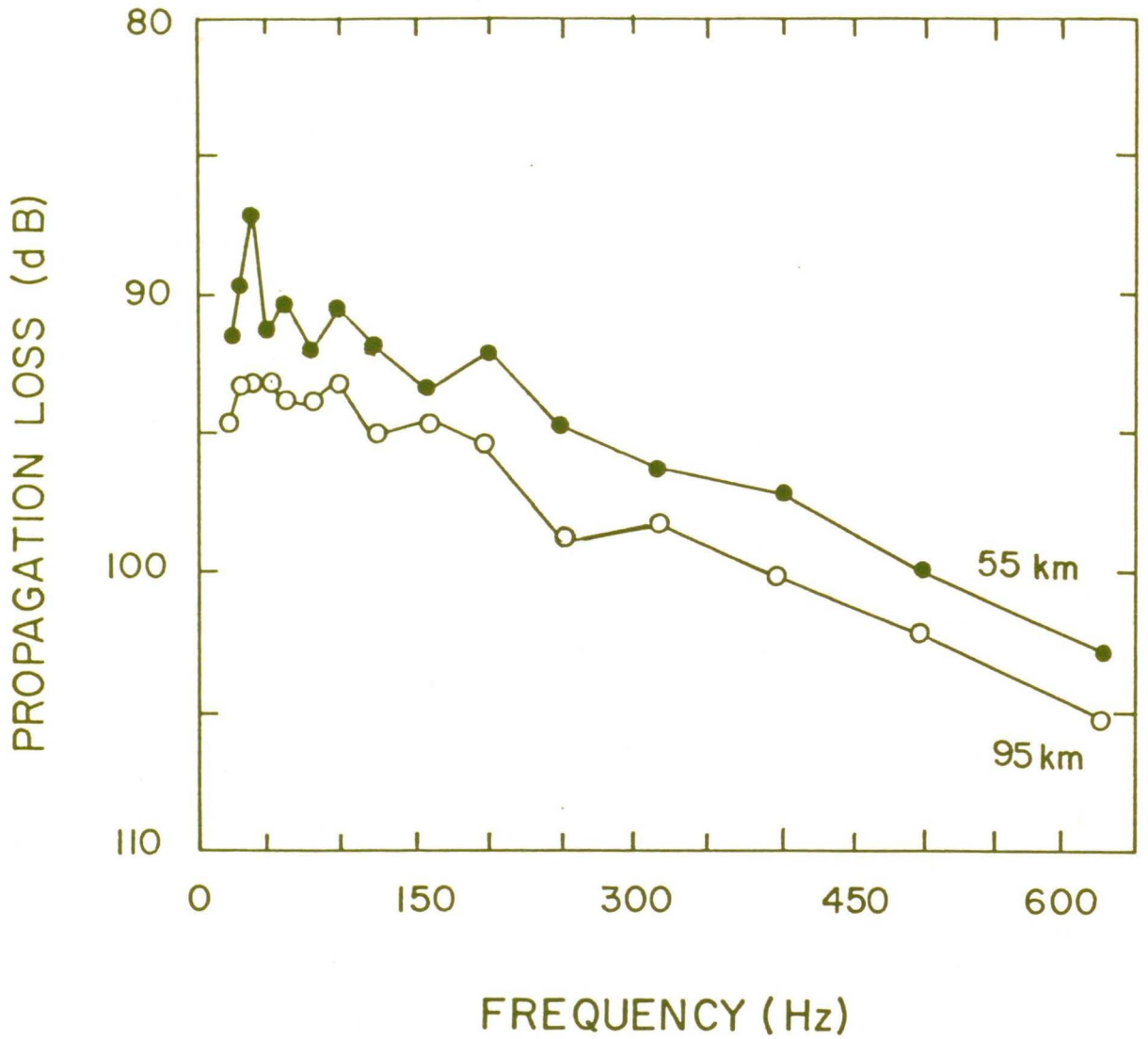


Fig. 3.14. Propagation loss as a function of frequency for sources at 55 and 95 km in range.

In Fig. 3.15 propagation loss is plotted as a function of range for 1/3-octave frequency bands centred at 25, 200, 400 and 630 Hz. The increase in propagation loss with frequency is also evident in this figure.

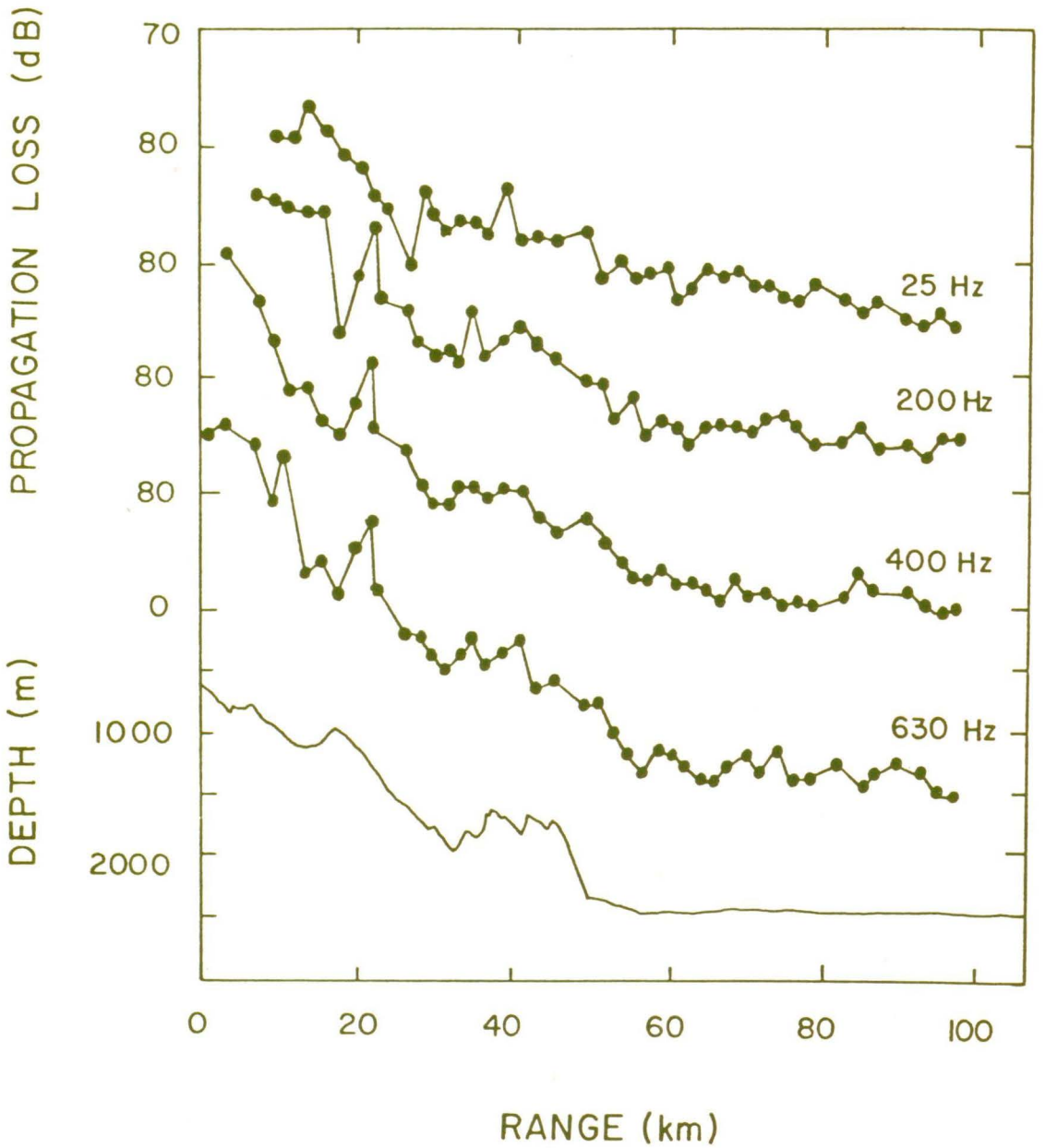


Fig. 3.15. Propagation loss as a function of range (bathymetry shown) for selected 1/3-octave bands centred at 25, 200, 400 and 630 Hz.

# CHAPTER 4
# THE PARABOLIC EQUATION METHOD

## 4.1 Introduction

In order to understand the nature of acoustic propagation in a particular environment, it is helpful to attempt to model the propagation loss of signal strength with range. This can be accomplished if the acoustic pressure field can be solved using the inhomogeneous wave equation for a realistic ocean environment. A direct solution of such a general formulation of the problem is, however, very difficult. One of the most promising techniques developed in recent years is the parabolic equation method (Spofford, 1973) which solves a parabolic approximation to the wave equation. The parabolic equation allows a non-iterative, "marching" type solution; that is, if an initial solution is known at some range r, the solution may be determined at a range $r+\Delta r$. The split-step Fourier method provides a fast, accurate algorithm to step the solution out in range.

The parabolic equation method is particularly applicable to modelling low-frequency sound propagation in a range-dependent environment, such as a continental slope region. In this respect it is quite distinct from the other main classes of approximations used: geometrical acoustics methods are valid only for high frequencies so that diffraction effects are negligible, while normal mode methods assume that the ocean is exactly stratified horizontally so that coupling between modes may be ignored. The model used in this thesis was developed by Thomson and Chapman (1983) specifically to consider wide-angle propagation paths, which can be important for the case of a sloping ocean bottom. Their model is extended in this thesis to include the effects of density variations in the sub-bottom layers.

The purpose of this chapter is to describe the parabolic equation method used to model numerically the acoustic propagation in a continental slope environment. In Section 4.2 the parabolic equation is derived beginning with the wave equation for an environment with constant density. In Section 4.3 the numerical solution of the parabolic equation is described, and in Section 4.4 the effects of variable density are considered.

## 4.2 Derivation of the Parabolic Equation

The acoustic pressure field in cylindrical coordinates, $\psi(r,z,\phi,t)$, due to a point source located at $r=0$, $z=z_s$ in a medium of constant density $\rho$ must satisfy the inhomogeneous wave equation

$$\nabla^2\psi - \frac{1}{c^2}\frac{\partial^2\psi}{\partial t^2} = -\frac{4\pi}{r}\psi_s\delta(r)\delta(z-z_s) \quad , \tag{4.1}$$

where $c = c(r,z,\phi)$ is the acoustic wave speed and $\psi_s$ is the source strength (the pressure at unit distance). Outside the immediate neighbourhood of the source, the source terms may be neglected and the corresponding homogeneous differential equation solved. Matching the solution in the far field to that near the source (the source modelling problem) will be considered in Section 4.3. With a simple harmonic time dependence,

$$\psi(r,z,\phi,t) = p(r,z,\phi)e^{-i\omega t} \quad , \tag{4.2}$$

where $\omega$ is the angular frequency, the wave equation reduces to

$$\nabla^2 p + \frac{\omega^2}{c^2}p = 0 \quad ,$$

or

$$\nabla^2 p + k_o^2 n^2 p = 0 \quad , \tag{4.3}$$

where $n(r,z,\phi) = \frac{c_o}{c(r,z,\phi)}$ is the acoustic refractive index and $c_o$ and $k_o = \frac{\omega}{c_o}$ are the reference wave speed and wave number, respectively. Jensen and Krol (1975) show that wave attenuation in the sub-bottom layers may be modelled by adding an imaginary part to the refractive index:

$$n^2 = (\frac{c_o}{c})^2 + i\frac{2\alpha c_o^2}{\omega c}$$

$$\approx (\frac{c_o}{c})^2 + i\frac{\beta}{27.287527}(\frac{c_o}{c})^2 \qquad (4.4)$$

where $\alpha = \alpha(r,z,\phi)$ is the attenuation per metre and $\beta = \beta(r,z,\phi)$ is the attenuation in dB/wavelength (dB/$\lambda$).

In a cylindrically symmetric environment, Eq. (4.3) may be written

$$\frac{\partial^2 p}{\partial r^2} + \frac{1}{r}\frac{\partial p}{\partial r} + \frac{\partial^2 p}{\partial z^2} + k_o^2 n^2 p = 0 \quad . \qquad (4.5)$$

This is the rotationally symmetric Helmholtz equation, an elliptic partial differential equation. In principle this equation could be solved directly as a boundary value problem. Boundary conditions are described by Tappert (1977), Jensen and Kuperman (1982) and Davis et al. (1982). The ocean surface boundary condition is that of vanishing pressure, assuming the density of air to be negligible compared to that of water. At the ocean floor, the balancing of forces across the ocean-ocean bottom interface requires that the particle velocity and pressure be continuous across the boundary. The radiation conditions $p \to 0$ as $z \to \infty$ and as $r \to \infty$ must also hold.

In practice a direct solution of Eq. (4.5) as a boundary value problem is very difficult since the complicated acoustic field must be solved in the entire two-dimensional region simultaneously (DeSanto, 1979). Fitzgerald (1975) shows that if the Helmholtz equation is solved as an initial value problem, the solutions are unstable because the second derivative $\frac{\partial^2}{\partial r^2}$ cannot distinguish between outward and inward propagating waves. In the parabolic equation method, the Helmholtz equation is approximated by a parabolic differential equation which is first order in r. This equation may be solved as an initial value problem and the solution marched out in range.

In the far field, the loss due to cylindrical spreading of the wavefront may be removed by the transformation

$$p(r,z) = \frac{1}{\sqrt{r}}\, u(r,z) \tag{4.6}$$

and Eq. (4.5) may be rewritten as

$$\frac{\partial^2 u}{\partial r^2} + \frac{\partial^2 u}{\partial z^2} + (k_o{}^2 n^2 + \frac{1}{4r^2})u = 0 \quad . \tag{4.7}$$

For such ranges $k_o n = \frac{\omega}{c} >> \frac{1}{r}$, which leads to the far field Helmholtz equation

$$\frac{\partial^2 u}{\partial r^2} + \frac{\partial^2 u}{\partial z^2} + k_o{}^2 n^2 u = 0 \quad . \tag{4.8}$$

Adopting the operator notation of Davis et al. (1982)

$$P = \frac{\partial}{\partial r}$$

$$Q = (n^2(r,z) + \frac{1}{k_o^2}\frac{\partial^2}{\partial z^2})^{1/2} \quad , \tag{4.9}$$

this equation may be written

$$(P^2+k_o^2Q^2)u = 0 \quad , \tag{4.10}$$

which may be factored as

$$(P+ik_oQ)(P-ik_oQ)u + ik_o[P,Q]u = 0 \quad . \tag{4.11}$$

Here $[P,Q]u = PQu - QPu$ is the commutator of the operators P and Q. For range-independent environments P and Q commute and $[P,Q] = 0$. In practice, for weakly range-dependent environments the commutator may be ignored (Thomson and Chapman, 1983) and Eq. (4.11) reduces to

$$(P+ik_oQ)(P-ik_oQ)u = 0 \quad . \tag{4.12}$$

The full solution to this equation is (Tappert, 1977)

$$u(r,z) = u_+(r,z) + u_-(r,z) \quad , \tag{4.13}$$

where $u_+$, the solution to $(P-ik_oQ)u_+ = 0$, is the outgoing wave and $u_-$, the solution to $(P+ik_oQ)u_- = 0$, is the incoming wave. In this approximation there is no coupling between $u_+$ and $u_-$ (range variations are necessary to couple outward and inward propagating waves) so if $u_-$ is zero initially, it will always remain zero. Then u(r,z) will represent an outgoing wave, the solution to

$$Pu = ik_oQu \quad . \tag{4.14}$$

Since Eq. (4.14) is first order in r, it is a differential equation of the parabolic type. For range-independent ocean environments it is exact for outgoing waves within the limits of the farfield approximation. For range-dependent environments, ignoring the commutator $[P,Q]u$ uncouples the outward and inward propagating waves, and thus all effects due to backscattering and reverberation are eliminated. This simplifies the formulation, but introduces an intrinsic error $[P,Q]u$ (Davis et al., 1982). Conditions under which this error is small have not been rigorously defined, although the problem has been considered by Claerbout (1976), Tappert (1977) and DeSanto (1977).

Equation (4.14) is the general parabolic equation. Although it represents a formal solution to the wave equation, its numerical implementation requires that the square root of the operator Q, defined by Eq. (4.9), must be specified. In practice, this can only be done approximately. Thomson and Chapman (1983) consider several split operator approximations to Q; two of these will be considered here.

The operator Q may be written

$$Q = (n^2(r,z) + \frac{1}{k_o^2}\frac{\partial^2}{\partial z^2})^{1/2}$$

$$= (1+\varepsilon+\mu)^{1/2} \quad , \tag{4.15}$$

where

$$\varepsilon = n^2(r,z)-1$$

$$\mu = \frac{1}{k_o^2}\frac{\partial^2}{\partial z^2} \quad . \tag{4.16}$$

Two possible approximations to Q are

$$Q_1 = 1 + \frac{1}{2}\epsilon + \frac{1}{2}\mu \tag{4.17}$$

and

$$Q_2 = (1+\mu)^{1/2} + [(1+\epsilon)^{1/2} - 1] \quad . \tag{4.18}$$

$Q_1$ is the standard approximation used widely in the study of ocean acoustics. It was obtained by Tappert and Hardin (Spofford, 1973) by expanding the operator Q in a binomial series and truncating after the second term. In order that this be a good approximation, the neglected terms must be small in the sense of some norm. Tappert (1977) defines an appropriate norm and demonstrates that this condition is met for small variations in the refractive index with depth and range and for small angles of propagation with respect to the horizontal. For long-range ocean wave-guide propagation (where repeated bottom interactions result in strong attenuation for the steep-angle paths) these requirements are generally satisfied and $Q_1$ represents an acceptable approximation.

The split-operator approximation $Q_2$ was developed in an attempt to extend the validity of the parabolic equation method to wider angles of propagation. It was originally presented by Feit and Fleck (1978) for the study of light propagation in optical fibers and was applied to acoustic propagation in the ocean by Thomson and Chapman (1983). They present a simple error analysis which demonstrates the improved accuracy of this approximation, particularly in cases involving wide angles of propagation and large variations in the refractive index. These improved capabilities are important in the study of acoustic interaction with a sloping ocean bottom where steep propagation paths can be significant.

## 4.3 Numerical Solution of the Parabolic Equation

The primary computational advantage of the parabolic equation is that, as a first order differential equation in r, it can be solved by a non-iterative, marching-type algorithm. This is accomplished by forming a numerical grid in range and depth and assuming a source distribution in z at some initial range. The acoustic field may then be marched out in range, requiring as input at each range step only the field at the previous range step and the environmental data. In this manner the acoustic field is calculated in the entire two-dimensional region. In this section the numerical solution of the parabolic equation, Eq. (4.14), using the wide-angle operator approximation $Q_2$ defined by Eq. (4.18) is briefly described following the work of Thomson and Chapman (1983).

For numerical calculations it is convenient to use the envelope transformation

$$u(r,z) = \Phi(r,z)e^{ik_o r}, \tag{4.19}$$

since for small $\mu$ the field $\Phi$ varies more slowly with range than u and thus can be solved on a coarser range grid. Substitution of Eqs. (4.18) and (4.19) into (4.14) leads to

$$P\Phi = ik_o(Q_2-1)\Phi \quad . \tag{4.20}$$

The operator identity (Thomson and Chapman, 1983)

$$(1+\mu)^{1/2} = 1 + \frac{\mu}{(1+\mu)^{1/2}+1}$$

allows this equation to be written as

$$P\underline{\Phi} = \frac{ik_o\mu}{(1+\mu)^{1/2}+1}\underline{\Phi} + ik_o(n-1)\underline{\Phi}$$

$$\text{or} \qquad \frac{\partial\underline{\Phi}}{\partial r} = i(A+B)\underline{\Phi} \quad , \tag{4.22}$$

where the operators A and B are defined

$$A = \frac{\frac{\partial^2}{\partial z^2}}{(k_o^2 + \frac{\partial^2}{\partial z^2})^{1/2}+k_o}$$

$$B = k_o[n(r,z)-1] \quad . \tag{4.23}$$

Equation (4.22) suggests that $\underline{\Phi}(r+\Delta r,z)$ may be approximated to $O(\Delta r^2)$ by

$$\begin{aligned}\underline{\Phi}(r+\Delta r,z) &= \underline{\Phi}(r,z) + \frac{\partial\underline{\Phi}}{\partial r}\Delta r \\ &= (1+i(A+B)\Delta r)\underline{\Phi}(r,z) \\ &= e^{i(A+B)\Delta r}\underline{\Phi}(r,z) \quad . \end{aligned} \tag{4.24}$$

The split-step method is implemented by approximating the exponential operator by (Tappert and Hardin, 1974)

$$e^{i(A+B)\Delta r} = e^{\frac{iA\Delta r}{2}} \cdot e^{iB\Delta r} \cdot e^{\frac{iA\Delta r}{2}} \quad , \tag{4.25}$$

and making use of the Fourier transform to calculate the z derivatives in $e^{\frac{iA\Delta r}{2}}$ (Thomson and Chapman, 1983). The resulting algorithm, correct to $O(\Delta r^2)$, is given by

$$\underline{\Phi}(r+\Delta r,z) = F^{-1}\{\exp\left[\frac{-ik_z^2\Delta r/2}{(k_o^2-k_z^2)^{1/2}+k_o}\right] \cdot F\{\exp(iB\Delta r) \cdot$$

$$F^{-1}\{\exp\left[\frac{-ik_z^2\Delta r/2}{(k_o^2-k_z^2)^{1/2}+k_o}\right] \cdot F\{\underline{\Phi}(r,z)\}\}\}\} \qquad (4.26)$$

where F denotes the discrete Fourier transform from z space to $k_z$ space and $F^{-1}$ denotes the inverse transform. Equation (4.26) defines the split-step Fourier solution for the parabolic equation. Although it is exact only for the case of constant refractive index n, McDaniel (1974) and Jensen and Krol (1975) show that when n is a function of r and z the solution is stable, and that by using small range steps $\Delta r$ and limiting the sound-speed gradients considered, the error in this approximation can be made arbitrarily small.

Although the parabolic equation as it has been formulated is not a boundary value equation, the boundary conditions can be included in the numerical implementation of the algorithm (Jensen and Krol, 1975; Davis et al., 1982). The ocean surface boundary condition of vanishing pressure can be included by taking an antisymmetric Fourier transform about the ocean surface; in practice this is accomplished by taking a fast sine transform. The conditions of continuity at the ocean floor can be simulated by extending the sound-speed profile into the bottom and including the velocity discontinuity at the interface. The radiation condition of $\underline{\Phi} \to 0$ as $z \to \infty$ can be approximated by adding an attenuating layer below the maximum depth of interest in the ocean bottom. Care must be taken that no significant energy exists at the bottom of this artificial absorbing layer. Jensen and Krol (1975) consider the numerical difficulties that can arise from truncating the pressure field in depth.

To initiate the split-step solution algorithm, the field $\Phi(r,z)$ must be known at some initial range r at all z values on the numerical grid. Several methods may be used to model this source distribution. If the ocean can be assumed to be exactly stratified near the source, the wave equation may be solved by normal mode methods and extended out several wavelengths to the region where the parabolic equation becomes valid. Jensen and Krol (1975) describe such a procedure. A simpler initial field based on a Gaussian distribution in z-space is described by Tappert (1977). For the numerical modelling in this thesis an initial field designed by Thomson (described in Davis et al., 1981 and Thomson and Chapman, 1983) was used. This source distribution has the advantage of requiring considerably less dense sampling than the standard Gaussian source.

## 4.4 The Variable-Density Parabolic Equation Model

In the previous sections, the parabolic approximation to the wave equation and the split-step Fourier solution have been presented for a constant density environment. Thomson and Chapman (1983) demonstrated excellent results in applying this model to ocean wave-guide problems. However, to model successfully acoustic interaction with the ocean bottom, the sub-bottom layers must be modelled as realistically as possible. Reflection and scattering due to abrupt changes in density between the ocean and the sub-bottom layers can be important. This section examines and tests a method of including the effects of changes in density in the parabolic equation model.

The reduced wave equation for acoustic pressure p in a medium of variable density $\rho$ is

$$\rho\nabla\cdot(\frac{1}{\rho}\nabla p) + \frac{\omega^2}{c^2}p = 0 \quad . \tag{4.27}$$

The transformation

$$q = \frac{p}{\sqrt{\rho}} \tag{4.28}$$

reduces this equation to the standard Helmholtz form

$$\nabla^2 q + k_o^2 n^2 q = 0 \quad , \tag{4.29}$$

where the "effective" index of refraction is now defined by (Tappert, 1977)

$$n^2 = \left(\frac{c_o}{c}\right)^2 + \frac{1}{2k_o^2}\left(\frac{1}{\rho}\nabla^2\rho - \frac{3}{2}\left(\frac{\nabla\rho}{\rho}\right)^2\right)$$

$$= \left(\frac{c_o}{c}\right)^2 + \frac{1}{2k_o^2}\rho^{1/2}\nabla\cdot(\rho^{-3/2}\nabla\rho) \quad . \tag{4.30}$$

With this definition of n (plus an imaginary part due to attenuation, if desired) the derivation and solution of the parabolic equation follow as before. However, large gradients in density can result in large changes in the effective index of refraction which violate the requirement that n be nearly constant in the parabolic equation method. For discontinuous changes in density occurring at the interface between two media, Tappert (1977) suggests an analytic expression for the density which smooths this transition:

$$\rho(z) = \frac{1}{2}(\rho_1+\rho_2) + \frac{1}{2}(\rho_2-\rho_1)\tanh\left(\frac{z-H}{L}\right) \quad , \tag{4.31}$$

where $\rho_1$ and $\rho_2$ are the densities of media 1 and 2, H is the depth of the interface, and L is the vertical distance over which the density changes. In order that the effects of this density change be modelled correctly and that large values of n be avoided, Tappert demonstrates that L must be chosen to satisfy

$$\frac{1}{k_o^2}\left|\frac{\rho_2-\rho_1}{\rho_2+\rho_1}\right| \ll L^2 \ll \frac{1}{k_o^2 \sin^2\theta}\,, \tag{4.32}$$

where $\theta$ is the angle of propagation with respect to the horizontal.

To verify that the effects of abrupt changes in density are modelled realistically, several test cases are considered. Test case 1, presented by Lee and Botseas (1982), consists of the range-independent, shallow water environment described in Fig. 4.1. The ocean bottom is simulated by a discontinuity of 5 m/s in the sound-speed profile and an abrupt change in density from 1.0 g/cm$^3$ to 2.1 g/cm$^3$.

In a range-independent environment, normal mode methods provide an exact solution (including all variable density effects) to the wave equation. For this test case the normal mode solution of Bucker (reported by Lee and Botseas, 1982) is used as a reference for the purposes of comparison. In Fig. 4.2 the propagation losses calculated using both the constant-density and variable-density parabolic equation models are compared with the reference normal mode solution. Figure 4.2(a) shows that the results obtained using the constant-density parabolic equation model differ considerably from the normal mode solution. However, including the effects of the density discontinuity according to Eqs. (4.30) - (4.32) leads to a significant improvement in the results, with Fig. 4.2(b) showing excellent agreement of the variable-density parabolic equation model results with the exact normal mode solution.

Test case 2, originally presented at the NORDA (Naval Ocean Research and Development Activity) Parabolic Equation Workshop (Davis et al., 1982), is designed to test how well abrupt changes in sound speed, density and attenuation can be modelled using the parabolic equation method. The environment, described in Fig. 4.3, consists of a 100-m deep, isovelocity ocean over an isovelocity bottom with discontinuities in sound speed, density and attenuation at the ocean floor. Two different

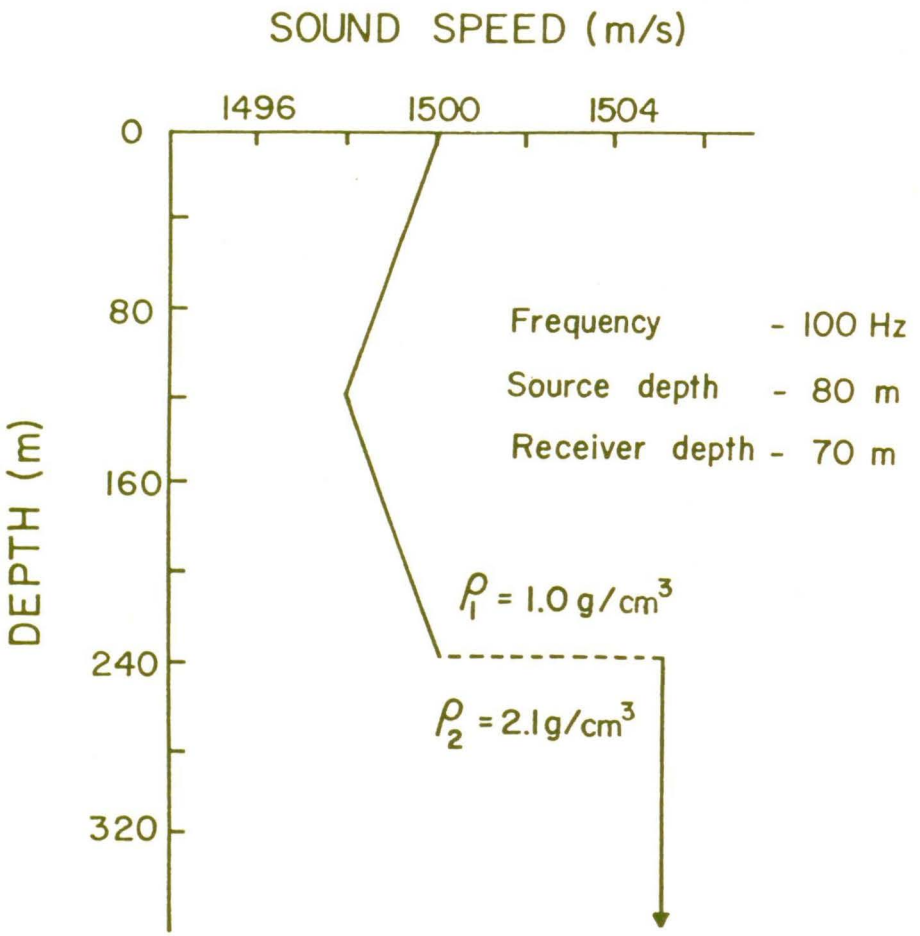


Fig. 4.1. Sound-speed profile and parameters for test case 1.

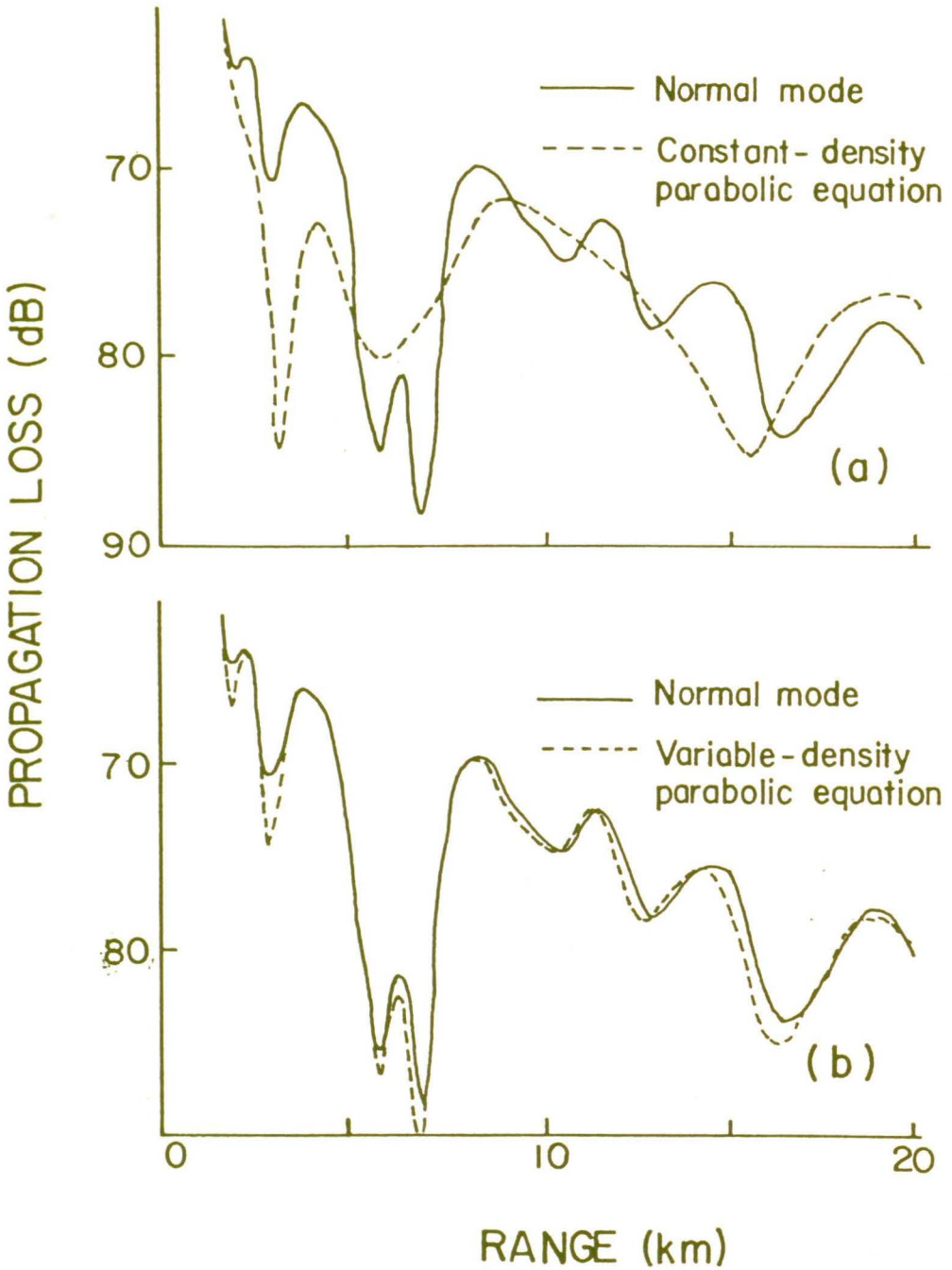


Fig. 4.2. Propagation loss as a function of range for test case 1 (Fig. 4.1) for the reference normal mode solution and for (a) the constant-density parabolic equation model, and (b) the variable-density parabolic equation model.

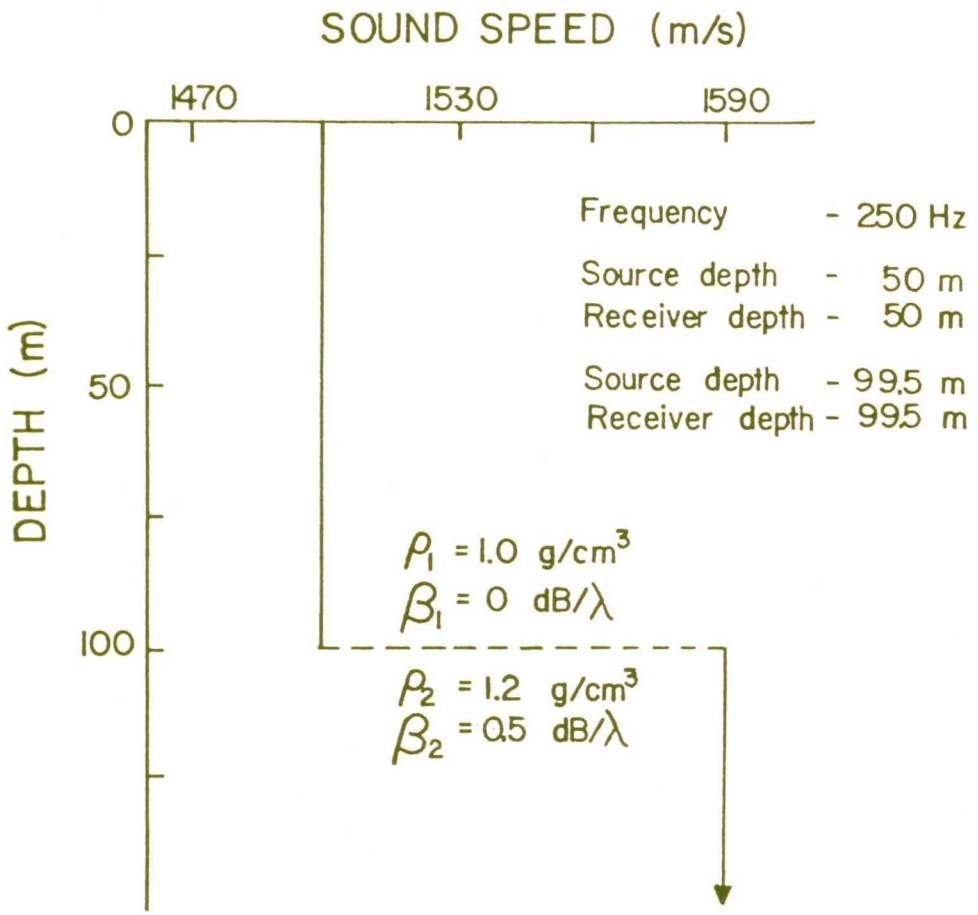


Fig. 4.3. Sound-speed profile and parameters for test cases 2A and 2B.

configurations of source and receiver depths are considered. Since the environment is range-independent, the parabolic equation model results may again be compared with an exact normal mode solution. For this test case the normal mode solution presented by Davis et al. (1982) is used as a reference.

The results of thirteen different parabolic equation models were compared at the NORDA workshop. In Fig. 4.4(a) (adapted from Davis et al., 1982), an envelope for the five best results presented at the workshop for range-dependent parabolic equation models are compared with the reference normal mode solution for the source and receiver both located at a depth of 50 m (test case 2A). The agreement in both level and phase is, in general, fairly good. However, Fig. 4.4(b) shows that significantly better results are obtained using the variable-density parabolic equation model described in this thesis. The propagation loss calculated using this model is essentially the same as the exact normal mode solution.

An even more challenging test of modelling acoustic interaction with the ocean bottom is to locate both the source and receiver at a depth of 99.5 m, just 0.5 m above the ocean floor (test case 2B). Figure 4.5(a) (adapted from Davis et al., 1982) shows an envelope for the three best results presented at the workshop for range-dependent parabolic equation models. These results differ significantly from the reference normal mode solution. However, the variable-density parabolic equation model calculations are again in excellent agreement with the exact normal mode solution, as shown in Fig. 4.5(b).

These test cases demonstrate that a valid treatment of the effects of density variations in the ocean bottom provides a significant contribution to modelling acoustic interaction with the ocean bottom. The excellent results obtained with the variable-density parabolic equation model indicate that it is a realistic propagation model for at least simple ocean environments.

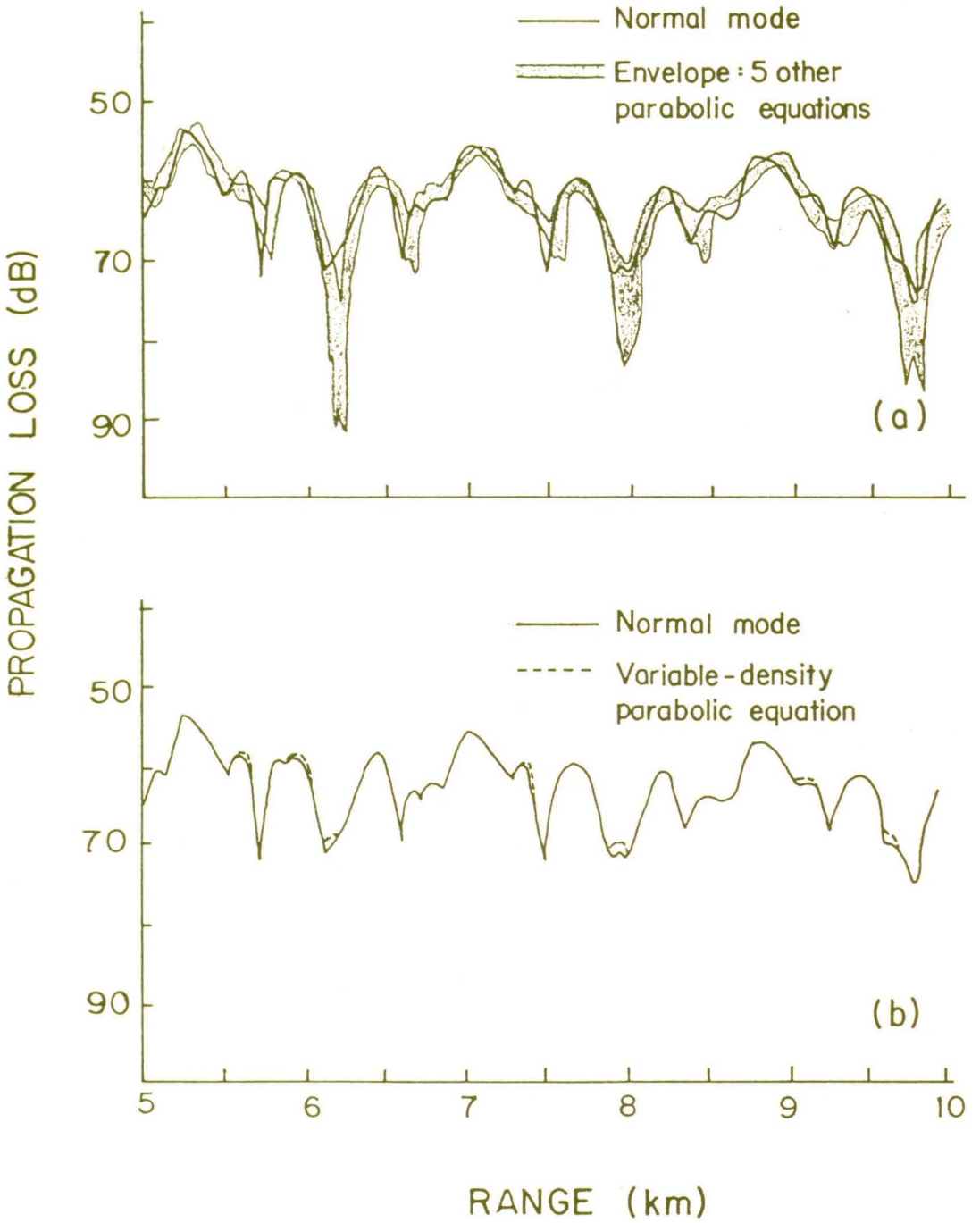


Fig. 4.4. Propagation loss as a function of range for test case 2A (Fig. 4.3) for the reference normal mode solution and for (a) an envelope of the 5 best parabolic equation results at the NORDA workshop (adapted from Davis et al, 1982) and (b) the variable-density parabolic equation model.

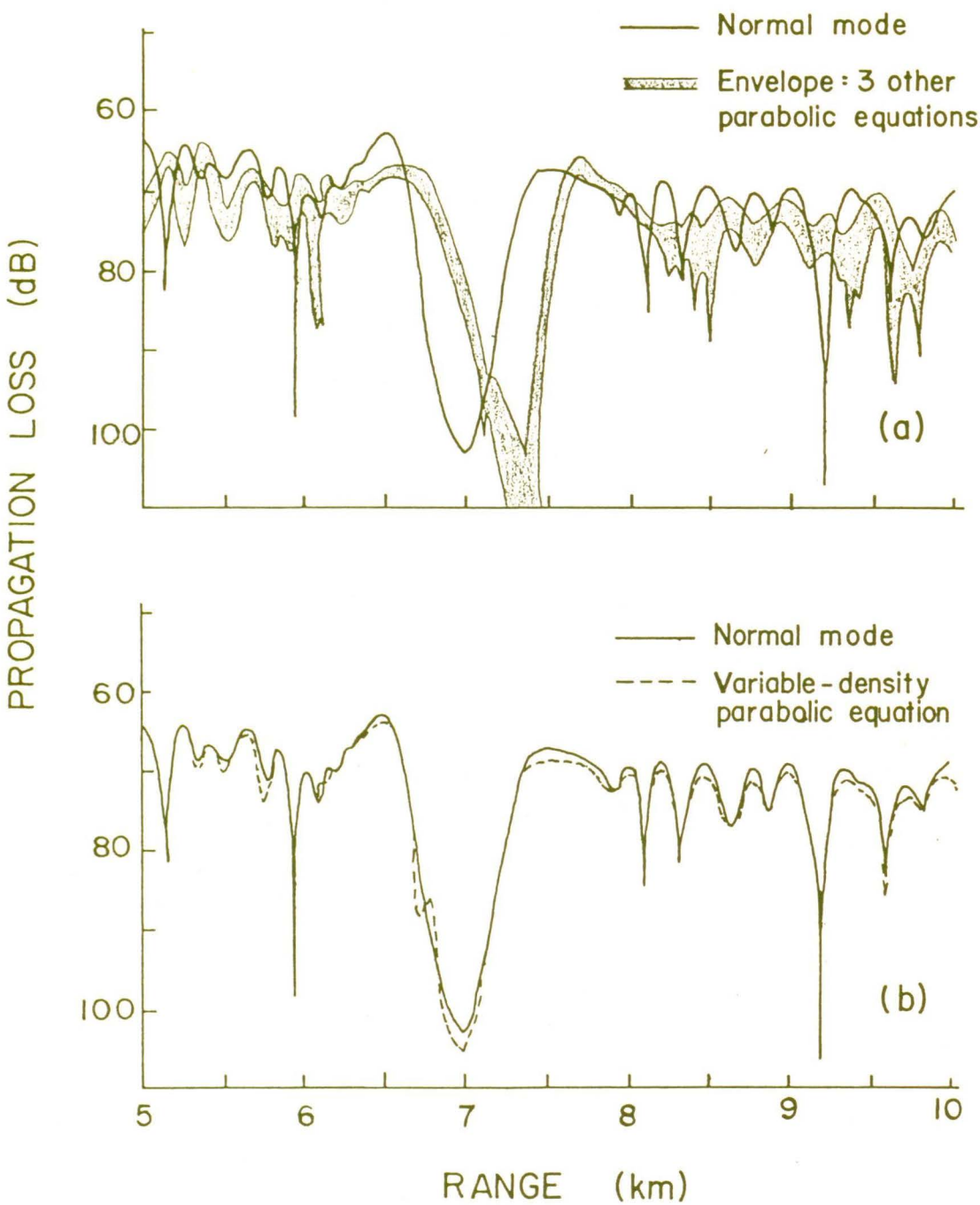


Fig. 4.5. Propagation loss as a function of range for test case 2B (Fig. 4.3) for the reference normal mode solution and (a) an envelope of the 3 best parabolic equation results at the NORDA workshop (adapted from Davis et al., 1982), and (b) the variable-density parabolic equation model.

# CHAPTER 5
# MODELLING PROPAGATION IN THE CONTINENTAL SLOPE ENVIRONMENT

## 5.1 The Downslope Propagation Model

Acoustic propagation in a continental slope environment is strongly influenced by the composition of the ocean-floor sediments and the variations in bathymetry with range. As described in Chapter 4, the variable-density parabolic equation method is particularly well-suited for modelling bottom-interacting propagation in a range-dependent environment. The purpose of this chapter is to present the results of modelling the downslope and upslope propagation measurements described in Chapter 3, using the variable-density parabolic equation model.

In order to model accurately the acoustic propagation in a particular ocean environment, it is important to represent the environment realistically. Some of the environmental parameters such as the sound speed in the water column and the bathymetry can be measured directly during the experiment. Other parameters such as the acoustic properties of the ocean bottom are more difficult or expensive to measure directly at sea. Values for these parameters can often be inferred from the acoustic measurements or determined from the existing geological records for the area of interest.

The ocean environment was represented by a three-layer model consisting of the water column, an underlying sediment layer and an absorbing substrate or basement. The sound-speed profiles and bathymetry of the water column were measured directly during shot run 1 and are shown in Fig. 3.1. The sound-speed structure in the ocean-floor sediment layer was determined for this shot run from an analysis of bottom reflectivity measurements using a deconvolution technique (Chapman, 1983b). This

technique, described by Chapman and Barrodale (1982) and Chapman et al. (1984), can be used to determine the ocean bottom impulse response to a depth of about 100-200 m below the ocean floor. The results of the study indicate a layer of unconsolidated sediments with an initial sound speed $c_0$ (at the ocean floor) of 1540 m/s and a (linear) sound-speed gradient g of 1.6 $s^{-1}$. No reflecting layers were detected within the sediments. These initial sediment sound-speed and gradient values suggest a clayey-silt composition, which is typical for a continental slope area where the sediments are mostly turbidites from terrestrial erosion (Hamilton, 1980). Hamilton reports that such sediments generally have a density of about 1.5 $g/cm^3$ and a compressional-wave attenuaton of about 0.1 dB/$\lambda$. Since the maximum sediment penetration depth in acoustical measurements for small explosive sources is about 100-150 m, the ocean bottom was modelled as a 150-m thick sediment layer (with the sound-speed structure, density and attenuation given above), overlying a semi-infinite absorbing basement, as shown in Fig. 5.1.

In the experiment, the receiver (hydrophone) was fixed and sources were detonated at selected range increments along the shot run track. However, numerical methods, such as the parabolic equation model, calculate the acoustic field throughout the environment due to a fixed source. Therefore, by the condition of reciprocity, the locations of source and receiver may be interchanged in the model: the source was placed at the (experimental) receiver location at a depth of 380 m, and the propagation loss was calculated for a depth of 22 m for the environmental model described above using the variable-density parabolic equation model. The model calculations are compared to the measured values for frequencies of 25, 200, 400 and 630 Hz in Fig. 5.2. To reduce the fluctuations due to interference effects at a single frequency, the model results were averaged over 2 km in range. These interference effects are smoothed out in the measured results due to the 1/3-octave band averaging in frequency.

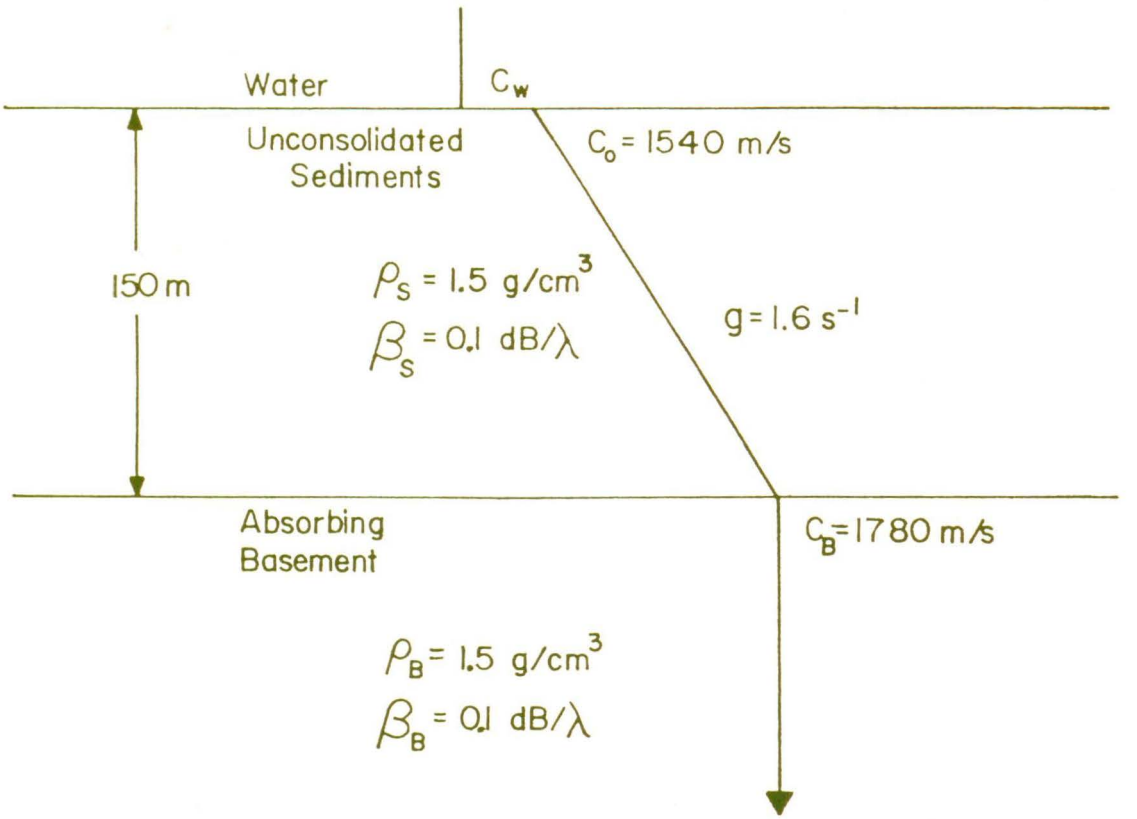


Fig. 5.1. The ocean bottom model for shot runs 1 and 2 (the heavy line indicates the sound-speed profile).

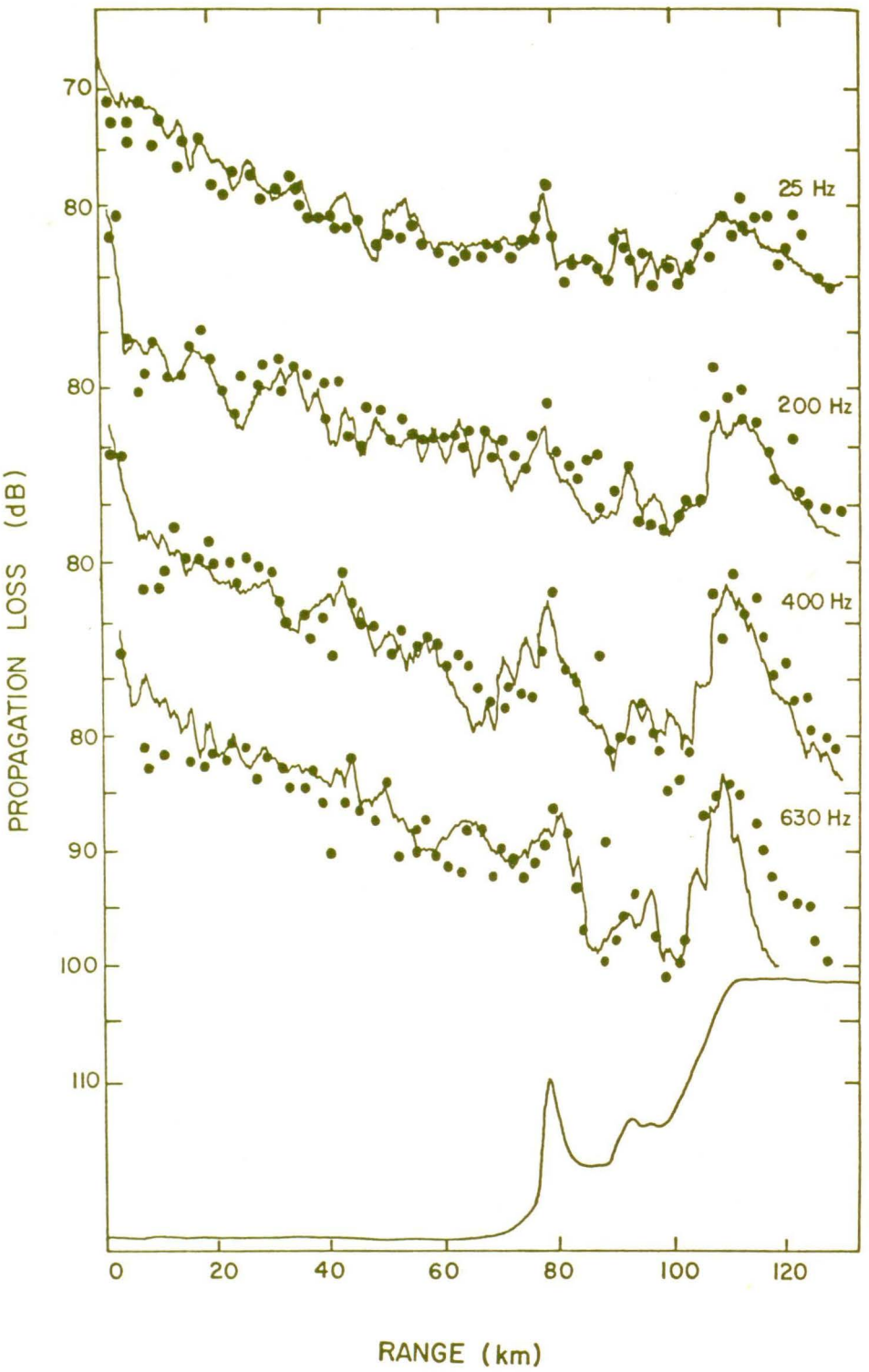


Fig. 5.2. Comparison of variable-density parabolic equation model results with measured propagation loss values (closed circles) for shot run 1 at frequencies of 25, 200, 400 and 630 Hz.

Figure 5.2 shows excellent agreement between the model calculations and the experimentally measured values. The propagation loss is modelled correctly in each of the three bathymetric regions along the track. The correct range-dependent behavior, including the slope enhancement effects at 75 and 110 km in range, is evident over the entire frequency band. The frequency dependence in each region also appears to be modelled correctly. In order to obtain good agreement at the higher frequencies, an increasingly fine numerical grid was required for the model calculations. The range and depth increments of the grid and L, the vertical distance over which the density change was implemented, are given for each frequency in Table 5.1. The practical high frequency limit of the model is approached at 630 Hz; at this frequency the steep-angle propagation which is important at short ranges (5-10 km) and in the continental shelf region (110-130 km) is not modelled adequately. However, the overall agreement between the model calculations and the measured values is excellent.

## 5.2 The Upslope Propagation Model

The comparison presented in Fig. 5.2 shows that accurate results can be obtained with the variable-density parabolic equation model if the environment is represented realistically. Unfortunately, no information on the acoustic properties of the ocean-floor sediments was available for the site of the upslope propagation shot run (shot run 2). Therefore, the ocean bottom model determined for shot run 1 (shown in Fig. 5.1) was also assumed to represent the ocean bottom along the track of shot run 2 in an attempt to model the propagation up the slope. The bathymetry and sound-speed structure in the water column were measured directly during the shot run and are shown in Fig. 3.9. By the condition of reciprocity, the source was placed at the (experimental) receiver location at a depth of 560 m, and the propagation loss was calculated for a depth of 22 m using the variable-

density parabolic equation model. The model calculations are compared to the measured values for frequencies of 25, 200, 400 and 630 Hz in Fig. 5.3. To reduce the fluctuations due to interference effects, the model results were averaged over 5 km in range. The numerical grid increments and density transition distances were the same as those used in the calculations for shot run 1, and are given in Table 5.1.

Figure 5.3 shows that although the range-dependent behavior appears to be modelled correctly (e.g. the rapid increase in loss at 0-25 and 45-55 km in range where the bottom slope is relatively regular and monatonic; the nearly constant loss from 55-95 km in range over the ocean basin) there are significant differences in level between the measured and calculated values. This would be expected for shot run 2, since the measured values include losses due to curvature out of the plane of propagation because the shot run track was not perpendicular to the contours of the slope (Fig. 2.2). A two-dimensional propagation model, such as the variable-density parabolic equation model, cannot account for these losses. If the sediment composition was known accurately, then a comparison of the measured and calculated losses could provide an estimate of this loss.

Table 5.1. Numerical grid increments (range and depth) and density transition distances used to model shot runs 1 and 2

| Frequency (Hz) | Range Increment (m) | Depth Increment (m) | Density Transition, L, (m) |
|---|---|---|---|
| 25 | 13 | 11 | 14 |
| 200 | 13 | 4 | 3.5 |
| 400 | 13 | 2 | 1.0 |
| 630 | 10 | 1.5 | 0.45 |

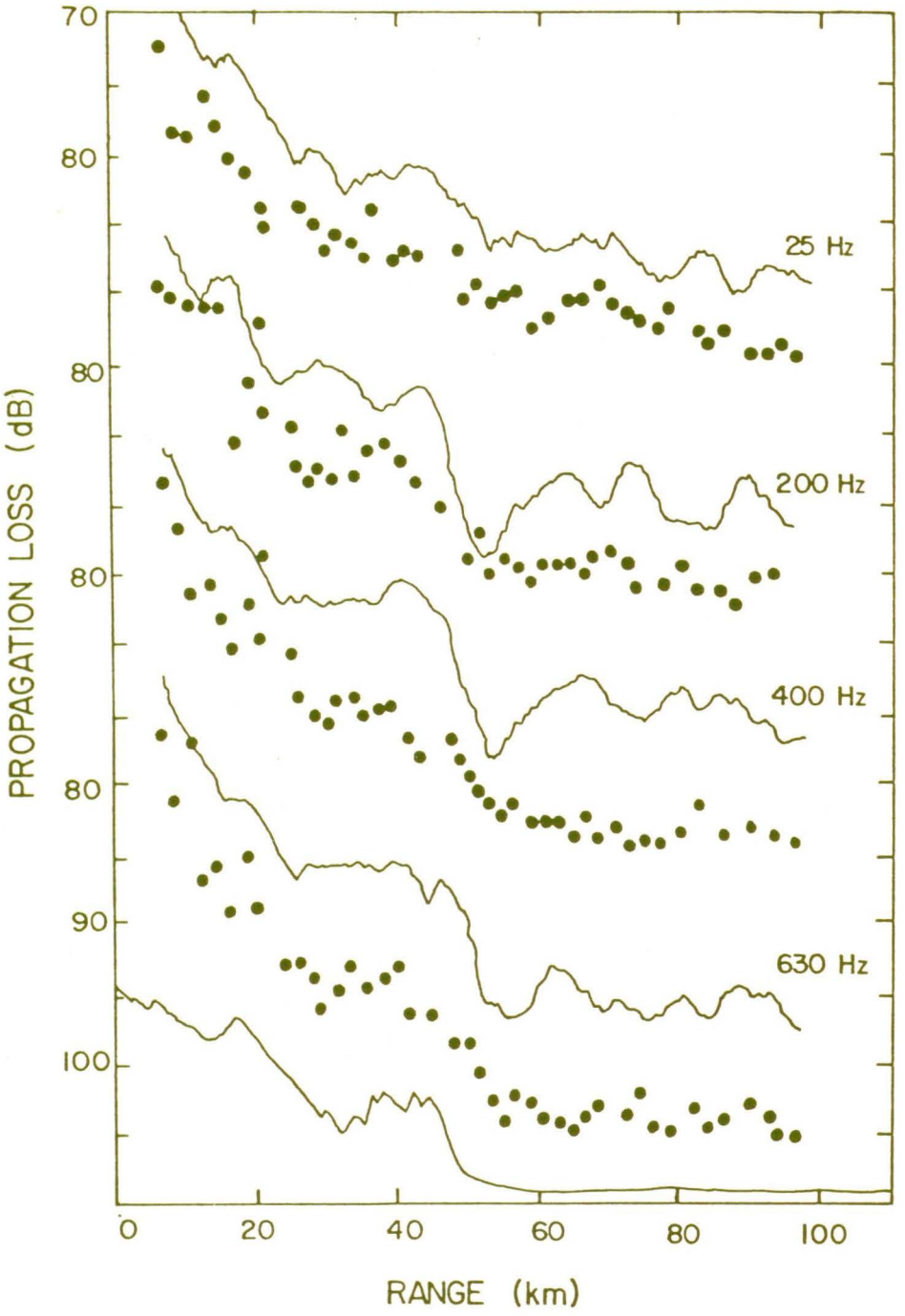


Fig. 5.3. Comparison of variable-density parabolic equation model results with measured propagation loss values (closed circles) for shot run 2 at frequencies of 25, 200, 400 and 630 Hz.

# CHAPTER 6
# SUMMARY

The purpose of the work reported in this thesis was to study acoustic propagation in a continental slope ocean environment. Experimental measurements of the propagation loss in 1/3-octave bands from 25 to 630 Hz were obtained for propagation both up and down the continental slope off the west coast of Vancouver Island, using a fixed array of hydrophones and explosive sound sources detonated at selected ranges. The propagation was strongly influenced by the ocean-floor bathymetry in the region of the source.

The track of the downslope propagation shot run included three distinct bathymetric regions: the deep ocean basin, the continental slope and the continental shelf. A slope enhancement effect (decreasing loss with range) was observed for sources located in the continental slope region. The maximum enhancement was recorded for sources near the edge of the continental shelf at ranges of about 110 km. The propagation loss measured for these sources was as much as 16 dB less than that estimated for propagation over a flat ocean bottom, and were equivalent to levels recorded for sources at 25-30 km in range over the deep ocean basin. This enhancement effect was explained in terms of acoustic ray theory: as the rays propagate down the slope, each bottom reflection reduces the ray angle by twice the slope angle and eventually the rays become continuously refracted within the deep sound channel and propagate without further bottom interactions. By this downslope conversion to low-loss paths, the propagation loss for a distant source located over a sloping ocean bottom is less than that for a nearer source located over a flat bottom. The sequence of arrivals and the frequency content of acoustic signals recorded

in each bathymetric region supported this analysis. Since the propagation loss due to bottom interactions increases with frequency, the slope enhancement effect was most pronounced at high frequencies.

The track of the upslope propagation shot run included two bathymetric regions: the continental slope and the deep ocean basin. The measured propagation loss increased rapidly with range for sources in the continental slope region: the loss measured for sources near the bottom of the slope (55 km in range) exceeded the estimated loss for a flat ocean bottom by as much as 15 dB. The propagation loss increased only gradually with range for sources in the deep ocean basin region. The excessive loss in the continental slope region was attributed to the steepening of the acoustic ray paths with each bottom reflection as the rays propagate up the slope. As the paths steepen, the rate of bottom interactions and the loss per interaction increases, resulting in a rapid increase in the propagation loss. The increase in the measured propagation loss with frequency indicated significant losses due to bottom interaction. Curvature of the ray paths out of the plane of propagation could also account for some of the loss, since the track of the upslope propagation shot run was not perpendicular to the contours of the slope.

In order to understand the nature of the acoustic propagation in a particular ocean environment, it is useful to model the propagation loss with range. The parabolic equation method, which solves a parabolic approximation to the wave equation, is well suited to modelling low-frequency propagation in a range-dependent environment. The model used in this thesis was developed by Thomson and Chapman (1983) to consider wide-angle propagation paths, which can be important for the case of a sloping ocean bottom. To model realistically the acoustic interaction with the ocean bottom, the model was extended in this thesis to include the effects of density variations in the sub-bottom layers. Several test cases

demonstrated that a valid treatment of the effects of density variations can lead to a significant improvement in predictions, and that the variable-density parabolic equation provides a realistic model of bottom-interacting acoustic propagation.

To model the acoustic propagation over the continental slope, the environment was represented by a three-layer model consisting of the water column, an underlying sediment layer and an absorbing basement. The sound-speed structure and bathymetry of the water column were measured directly during the experiment. For the downslope propagation shot run the sound-speed structure of the sediment layer was available from a previous analysis of bottom-reflectivity measurements. The sediment composition was identified as a clayey-silt from these parameters, and the density and attenuation were determined for this sediment type from geological records. The absorbing basement was placed at the maximum depth of acoustic penetration in the sediments. The losses calculated for propagation down the slope were in excellent agreement with the experimentally measured values over the entire frequency band of the measurements, indicating that the variable-density parabolic equation method can model propagation over the continental slope accurately when the environment is represented realistically.

Since no information on sediment composition was available for the upslope propagation shot run, the ocean bottom layers were modelled as for the downslope case. The losses calculated for propagation up the slope exhibited the correct range-dependent behavior, but differed in level from the measured values. A difference would be expected since the measured values include losses due to curvature out of the plane of propagation, which cannot be accounted for by a two-dimensional model. If the sediment composition was known accurately, then a comparison of the measured and calculated losses could provide an estimate of this loss.

## REFERENCES

Buckingham, M.J. 1983. Acoustic Propagation in a Wedge-shaped Ocean. In: Acoustics and the Sea-Bed. N.G. Pace, ed. Bath University Press, 251-159.

Chapman, N.R. 1983a, Modeling ocean bottom reflection loss measurements with the plane wave reflection coefficient. J. Acoust. Soc. Am. 73, 1601-1607.

Chapman, N.R. 1983b. unpublished data.

Chapman, N.R. and Barrodale, I. 1983. Deconvolution of marine seismic data using the $l_1$ norm. Geophys. J.R. astr. Soc. 72, 93-100.

Chapman, N.R., Barrodale, I. and Zala, C.A. 1984. Measurement of Sound-Speed Gradients in Deep-Ocean Sediments Using $l_1$ Deconvolution Techniques. IEEE Journal of Oceanic Engineering. OE-9, No. 1, 26-30.

Chapman, N.R., Zelt, C.A. and Busch, A.E. 1983. Geoacoustic modelling of deep water abyssal plains. In: Acoustics and the Sea-Bed. N.G. Pace, ed., Bath University Press, 297-305.

Christensen, R.E. Frank, J.A. and Geddes, W.H. 1975. Low frequency propagation via shallow refracted paths through deep ocean unconsolidated sediments. J. Acoust. Soc. Am. 57, 1421-1426.

Claerbout, J.F. 1976. Fundamentals of Geophysical Data Processing. McGraw-Hill Book Company.

Cornyn, J.J. 1973a. GRASS: A Digital-Computer Ray-Tracing and Transmission-Loss-Prediction System. Volume I - Overall Description. Nav. Res. Lab. Rept 7621.

Cornyn, J.J. 1973b. GRASS: A Digital-Computer Ray-Tracing and Transmission-Loss-Prediction System. Volume II - Users Manual. Nav. Res. Lab. Rept. 7642.

Davis, J.A., White, D. and Cavanagh, R.C. 1982. NORDA Parabolic Equation Workshop, 31 March-3 April 1981. NORDA Tech. Note 143. Naval Ocean Research and Development Activity, NSTL Station, Ms.

DeSanto, J.A. 1977. Relations between the solution of the Helmholtz and parabolic equations for sound propagation. J. Acoust. Soc. Am. 62, 295-297.

DeSanto, J.A. 1979. Theoretical methods in ocean acoustics. In: Ocean Acoustics. J.A. DeSanto, ed. Springer-Verlag, 7-77.

Dosso, S.E. and Chapman, N.R. 1983. Acoustic propagation in a shallow sound channel in the Northeast Pacific Ocean. J. Acoust. Soc. Am. 75, 413-418.

Ewing, M. and Worzel, J.L. 1948. Long Range Sound Transmission. Geological Soc. of America Memoir 27.

Feit, M.D. and Fleck, J.A. 1978. Light propagation in graded-index fibers. Appl. Opt. 17, 3990-3998.

Fitzgerald, R.M. 1975. Helmholtz equation as an initial value problem with application to acoustic propagation. J. Acoust. Soc. Am. 57, 839-842.

Gilbert, K.E., Evans, R.B., Chin-Bin, S.A., White, D. and Kuperman, W.A. 1983. Bottom-limited Ocean Environments. In: Acoustics and the Sea-Bed. N.G. Pace, ed. Bath University Press. 243-250.

Graves, R.D., Nagal, A. and Überall, H. 1975. Range-dependent normal modes in underwater sound propagation: Application to the wedge-shaped ocean. J. Acoust. Soc. Am. 58. 1171-1177.

Hamilton, E.L. 1980. Geoacoustic modeling of the sea floor. J. Acoust. Soc. Am. 68. 1313-1333.

Harrison, C.H. 1977. Three-dimensional ray paths in basins, troughs, and near seamounts by use of ray invariants. J. Acoust. Soc. Am. 62, 1382-1388.

Hoffman, A.P. and Thomson, D.J. 1978. Implementation of the GRASS model on the DREP Sigma 7 Computer. DREP Lab. Note 78-8. Defence Research Establishment Pacific, Esquimalt, B.C.

Jensen, F.B. and Krol. H. 1975. The use of the parabolic equation method in sound propagation modelling. SACLANTCEN Memo. SM-72. Saclant ASW Research Centre, La Spezia, Italy.

Jensen, F.B. and Kuperman, W.A. 1975. Consistency tests of acoustic propagation models. SACLANTCEN Memo. SM-157. Saclant ASW Research Centre, La Spezia, Italy.

Jensen, F.B. and Kuperman, W.A. 1980. Sound propagation in a wedge-shaped ocean with a penetrable bottom. J. Acoust. Soc. Am. 67, 1564-1566.

Klein, E. 1968. Underwater Sound and Naval Research and Applications before 1939. J. Acoust. Soc. Am. 43, 931-947.

Koch, R.A. 1983. Underwater Acoustic Propagation Dependence on Sediment Type for a Sloping Bottom. In: Acoustics and the Sea-Bed. N.G. Pace, ed. Bath University Press, 261-269.

Koch, R.A. Rutherford, S.R. and Payne, S.G. 1983. Slope propagation: Mechanisms and parameters sensitivities. J. Acoust. Soc. Am. 74, 210-218.

Lasky, M. 1976. Review of undersea acoustics to 1950. J. Acoust. Soc. Am. 61, 283-297.

Lee, D. and Botseas, G. 1982. IFD: An Implicit Finite-Difference Computer Model for Solving the Parabolic Equation. NUSC Technical Report 6659. Naval Underwater Systems Centre, New London, Conn.

Lichte, H. 1919. On the Influence of Horizontal Temperature Layers in Sea Water on the Range of Underwater Sound Signals. Physik, 17, 385. Translated by A.F. Wittenborn.

Northrop, J., Lougbridge, M.S. and Werner, E.W. 1968. Effects of near-source bottom conditions on long range sound propagation in the ocean. J. GEO. Res. 73, 3905-3908.

Officer, C.B. 1958. Introduction to the Theory of Sound Transmission with Application to the Ocean. McGraw-Hill Book Company.

Sommerfeld, A. 1894. Zur analytischen theorie der Warmeleitung. Math Ann. 45, 263-277.

Sommerfeld, A. 1896. Mathematische theorie der diffraction. Math. Ann. 47, 317-374.

Spofford, C.W. 1973. Synopsis of the AESD workshop on acoustic-propagation modelling by non-ray tracing techniques, 22-25, May 1973. AESD TN 73-05. Acoustic Environmental System Development, Arlington, Va.

Stifler, W.W. and Saars, W.F. 1948. Sofar. Electron. 21, 98.

Tappert, F.D. and Hardin, R.H. 1974. Proc. 8th Intern. Cong. on Acoustics. Goldcrest, London.

Tappert, F.D. 1977. The Parabolic Approximation Method. In: Wave Propagation and Underwater Acoustics. Joseph B. Keller and John S. Papadakis, ed. Springer-Verlag, 224-287.

Thomson, D.J. and Chapman, N.R. 1983. A wide-angle split-step algorithm for the parabolic equation. J. Acoust. Soc. Am. 74, 1848-1854.

Urick, R.J. 1982. Sound Propagation in the sea. Peninsula Publishing.

# VITA

Surname: DOSSO Given Names: STANLEY EDWARD

Place of Birth: Victoria, B.C. Date of Birth: December 6, 1959

Educational Institutions Attended:

UNIVERSITY OF VICTORIA 1977-1985

Degrees, Diplomas, Etc., Awarded:

| | | |
|---|---|---|
| BSc (Honours) | 1982 | University of Victoria |
| MSc (anticipated) | 1985 | University of Victoria |

Honours and Awards:

| | | |
|---|---|---|
| Prov. of British Columbia Grade 12 Scholarship | 1977/78 | |
| President's Entrance Scholarship | 1977/78 | University of Victoria |
| Wood's Trust Scholarship | 1978/79 | University of Victoria |
| President's Scholarship | 1978/79 | University of Victoria |
| R.T. Wallace Commemorative Scholarship | 1979/80 | University of Victoria |
| Hazel T. Knox Memorial Scholarship | 1980/81 | University of Victoria |
| B.W. Pearse Science Scholarship in Mathematics | 1980/81 | University of Victoria |

| | | |
|---|---|---|
| Eligible for President's Scholarship but could not accept due to awards already held | 1980/81<br>1981/82 | University of Victoria |
| B.W. Pearse Science Scholarship | 1981/82 | University of Victoria |
| Robert S. Evans Scholarship | 1981/82 | University of Victoria |
| The University of Victoria Jubilee Medal | 1982 | University of Victoria |
| The R.M. Pearce Memorial Fellowship | 1984/85 | University of Victoria |
| N.S.E.R.C. Post Graduate Scholarship | 1983/84<br>1984/85 | |

Publications:

Dosso, S.E. and Chapman, N.R. 1984. Acoustic propagation in a shallow sound channel in the Northeast Pacific Ocean. J. Acoust. Soc. Am. 75, 413-418.

Dosso, S.E. 1983. Implementation of the SNAP model on the DREP Sigma 7 Computer. DREP Lab. Note 83-2. Defence Research Establishment Pacific, Victoria, B.C.

Papers Presented at Scientific Meetings:

Dosso, S.E. and Chapman, N.R. 1983. Acoustic Propagation in a Shallow Sound Channel. Canadian Acoustical Association Meeting at Vancouver, B.C.

PARTIAL COPYRIGHT LICENCE

I hereby grant the right to lend my thesis (the title of which is shown below) to users of the University Library, and to make single copies only for such users or in response to a request from the library or any other university, or similar institution, on its behalf or for any of its users. I further agree that permission for extensive copying of this thesis for scholarly purposes may be granted by me or a member of the University designated by me. It is understood that copying or publication of this thesis for financial gain shall not be allowed without my written permission.

Title of Thesis:

ACOUSTIC PROPAGATION IN A CONTINENTAL SLOPE OCEAN ENVIRONMENT

Author [redacted]

Signature

Stanley Edward Dosso

April 16/1985

Date